GeoScienceWorld
Lithosphere
Volume 2023, Article ID lithosphere_2023_190, 21 pages
https://doi.org/10.2113/2023/lithosphere_2023_190

Lithosphere

Research Article

Mesozoic-Cenozoic Topographic Evolution of the South Tianshan (NW China): Insights from Detrital Apatite Geo-Thermochronological and Geochemical Analyses

Dunfeng Xiang,[1,2,3] Zhiyong Zhang,[1] David Chew,[3] Marc Jolivet,[4] Marco G. Malusà,[5] Chao Guo,[1] Nan Wang,[1] and Wenjiao Xiao[2]

[1]*State Key Laboratory of Lithospheric Evolution, Institute of Geology and Geophysics, Chinese Academy of Sciences, Beijing 100029, China*
[2]*Xinjiang Research Center for Mineral Resources, Xinjiang Institute of Ecology and Geography, Chinese Academy of Sciences, Urumgi 830011, China*
[3]*Department of Geology, School of Natural Sciences, Trinity College, Dublin 2, Ireland*
[4]*Univ Rennes, CNRS, Géosciences Rennes, UMR 6118, CNRS, F-35000 Rennes, France*
[5]*Department of Earth and Environmental Sciences, University of Milano-Bicocca, Milano 20126, Italy*

Correspondence should be addressed to Zhiyong Zhang; zyzhang@mail.iggcas.ac.cn

Received 9 May 2023; Accepted 14 July 2023; Published 15 September 2023

Academic Editor: Xiaoming Shen

The present-day topography of Tianshan is the product of repeated phases of Meso-Cenozoic intracontinental deformation and reactivation, whereas the long-term Mesozoic topographic evolution and the timing of the onset of Cenozoic deformation remain debated. New insights into the Meso-Cenozoic geodynamic evolution and related basin-range interactions in the Tianshan were obtained based on new detrital single-grain apatite U-Pb, fission-track, and trace-element provenance data from Mesozoic sedimentary sequences on the northern margin of the Tarim Basin. Detrital apatite U-Pb age data from Early-Middle Triassic clastic rocks show two prominent age populations at 500–390 Ma and 330–260 Ma, with a paucity of ages between 390 and 330 Ma, suggesting that sediment source is predominantly from the northern Tarim and South Tianshan. From the Late Triassic to Early Jurassic, the first appearance of populations in the 390–330 Ma and 260–220 age ranges indicates that the Central Tianshan-Yili Block and Western Kunlun Orogen were source regions for the northern margin of Tarim Basin. In the Cretaceous strata, south-directed paleocurrents combined with the decrease in the 390–330 Ma age population from the Central Tianshan-Yili Block imply that South Tianshan was uplifted and again became the main source region to the Baicheng-Kuqa depression during the Cretaceous. Our new apatite fission-track data from the southern Chinese Tianshan suggest that rapid cooling commenced at c. 30 Ma along the southern margin, and the Early Mesozoic strata exposed on the southern flank of the Tianshan underwent c. 4–5 km of late Cenozoic exhumation during this period. This age is approximately synchronous with the onset of exhumation/deformation not only in the whole Tianshan but also in the interior of the Tibetan Plateau and its margins. It suggests that far-field, N-directed shortening resulting from the India-Asia collision was transmitted to the Tianshan at that time.

1. Introduction

The geological evolution of the Tianshan Range attests to a complex history of long-lived accretion and continental growth in the Paleozoic, a long period of peneplanation in the Mesozoic, and later phases of Meso-Cenozoic reactivation caused by accretionary and collisional events along the Eurasian margin [1–4]. In contrast to the well-studied pre-Mesozoic and Cenozoic history of the Chinese Tianshan, its Mesozoic tectono-geomorphological evolution

and the genesis of its basin-and-range system remain controversial. For example, some studies have suggested that the basins on both sides of the Chinese Tianshan Range have been foreland basins since the Mesozoic [5–8], whereas others argued that the Tianshan Range and its related basin systems have been under an extensional regime associated with post-orogenic extension following Late Paleozoic collision [9, 10]. In addition, compared with the well-established source-to-sink relationships between the Pamir-Tianshan and the western Tarim Basin, the source-to-sink evolution between the Western Kunlun Orogen and the eastern Tarim Basin during the Mesozoic is more uncertain due to the limited amount of detrital single-grain age data [11].

Fortunately, Mesozoic sediments in the basins adjacent to and within the Tianshan orogen can provide constraints on its geological evolution. Among them, the Baicheng-Kuqa depression, located within the Tarim Basin, preserves a continuous late Paleozoic to Cenozoic sedimentary record with only minor hiatuses [12]. Provenance studies of these clastic sediments are important for paleogeographic and tectonic reconstructions of the Tianshan orogen. Detrital zircon U-Pb dating has proven to be a powerful tool for provenance constraints and paleo-drainage reconstructions in sedimentary basins adjacent to mountain belts [11, 13]. However, detrital zircon U-Pb data interpretations can be challenging due to recycling and the bias of zircon toward felsic igneous sources. Unlike the commonly employed detrital zircon U-Pb chronometer, apatite is a ubiquitous accessory mineral in all common crystalline rocks and therefore preserves information from a wide spectrum of sources [14, 15]. Furthermore, apatite trace element data can discriminate its source rock composition [16]. Combining age and trace element composition, detrital apatite can therefore be employed to make highly specific provenance determinations. This study presents the first detrital apatite U-Pb and trace element data from the Mesozoic sedimentary units in the Baicheng-Kuqa depression. The results shed light on the source-to-sink evolution of the Chinese South Tianshan (STS) during the Mesozoic.

In addition, apatite fission-track (AFT) age – stratigraphic depth profiles within sedimentary successions in foreland basins can provide information on the timing and amount of burial/exhumation of the basin, which in turn may have implications for the timing of uplift and erosional unroofing of the hinterland [17]. We also carried out AFT analysis on the same grains in these samples from Mesozoic sandstones exposed on the southern flank of the Tianshan in order to better constrain the onset of exhumation in the southern Chinese Tianshan during the Cenozoic.

2. Geological Setting and Mesozoic Stratigraphic Characteristics

The Tianshan Orogen forms the southwestern extremity of the Central Asian Orogenic Belt and includes the Kyrgyz Tianshan and the Chinese Tianshan. The Chinese sector of the Tianshan orogen is divided into the Eastern and Western Tianshan segments by the line of longitude at c. 88°E. This study focuses mainly on the Chinese Western Tianshan, Kyrgyz Tianshan, and Pamir, with a longitude range of c. 70°E–90°E (Figure 1(a)). This region is subdivided into the North Tianshan Belt (NST), the Central Tianshan-Yili Block (CTS-YL), and the STS by two major faults (the North Tianshan Fault and the South Nalati Fault, respectively; Figure 1(b), Reference 11).

The North Tianshan belt is interpreted as a late Paleozoic accretionary complex in which Precambrian basement is absent (Figure 1(b)) [18]. The Yili Block and Central Tianshan Block are two microcontinental blocks with Precambrian metamorphic rocks overlain by Phanerozoic sedimentary and volcanic successions. Finally, the STS orogenic belt is considered as a complex orogenic belt composed of continental basement, Palaeozoic marine sedimentary rocks, ophiolitic mélanges, and high to ultrahigh-pressure metamorphic rocks (Figure 1(b)) [3, 19]. The Tarim Craton, located adjacent to the STS, is one of the largest Precambrian continental blocks in China.

Following Paleozoic accretionary orogenesis, over 10 km of terrestrial Mesozoic and Cenozoic sediments were deposited in the basins in front of the Chinese West Tianshan orogen (Junggar and Tarim basins) [20]. Clastic sediments with a thickness of 6–8 km were deposited in the Baicheng-Kuqa depression of the Tarim Basin during the Meso-Cenozoic [12, 20]. This study focuses on the Kapushaliang region in the Baicheng-Kuqa depression as it has exceptional preservation and exposure of the Mesozoic sedimentary succession (Figure 2(a)). The Mesozoic sequences include the Lower to Middle Triassic Ehuobulake Group ($T_{1\text{-}2eh}$); the Middle to Upper Triassic Misibulake Group ($T_{2\text{-}3ms}$); the Lower Jurassic Taliqike (J_{1t}) and Ahe (J_{1a}) formations; the Middle Jurassic Yangxia (J_{2y}), Kenuzierle (J_{2k}), and Qiketai (J_{2q}) formations; the Upper Jurassic Qiakemake Group (J_{3qk}); the Lower Cretaceous Yageliemu (K_{1y}), Shushanhe (K_{1s}), and Baxigai (K_{1b}) formations; and the Upper Cretaceous Bashijiqike Formation (K_{2b}; Figure 2(b)) [21].

Three depositional hiatuses are observed at the boundaries between the Upper Permian and Lower Triassic, Upper Jurassic and Lower Cretaceous, and Lower Cretaceous and Paleogene [12, 21]. The Early Triassic succession represents gravels laid down in a braided river-alluvial plain environment, while the Middle-Late Triassic series was characterized by fluvial delta-lacustrine depositional systems [22]. Abundant coal in the Lower and Middle Jurassic strata indicates meandering fluvial and lacustrine depositional environments influenced by wet paleoclimate associated with monsoonal circulation [5, 12], whereas purple-red argillaceous siltstones of the uppermost Jurassic sequence (Qiakemake Group) suggest a relatively dry and hot environment. The Cretaceous sequence begins with a 20–30 m thick red conglomerate grading into coarse- to medium-grained sandstone, reflecting alluvial fan deposits transitioning into braided river-lacustrine facies clastic sediments [21]. The regional stratigraphic column and brief descriptions for each unit are presented in Figure 3.

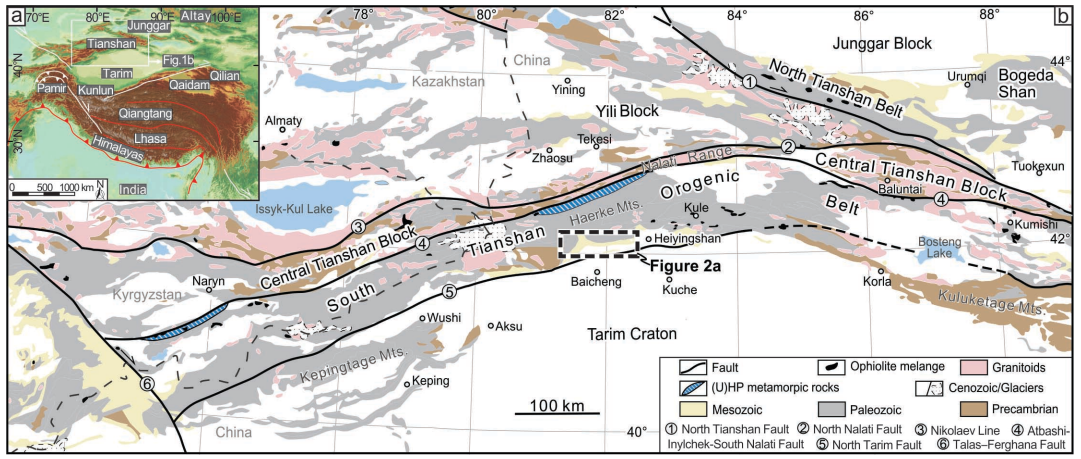

FIGURE 1: (a) Topographic map of the Tarim Craton, Tibetan Plateau, and Tianshan (modified after References 100, 101). White solid lines represent major faults, whereas red lines indicate suture zones in the Tibetan Plateau. The white box indicates the area depicted in b. (b) Schematic geological map of the northern part of the Tarim Craton and the Tianshan Range (modified after References 11, 20). The area outlining the map in Figure 2(a) is highlighted by a rectangle.

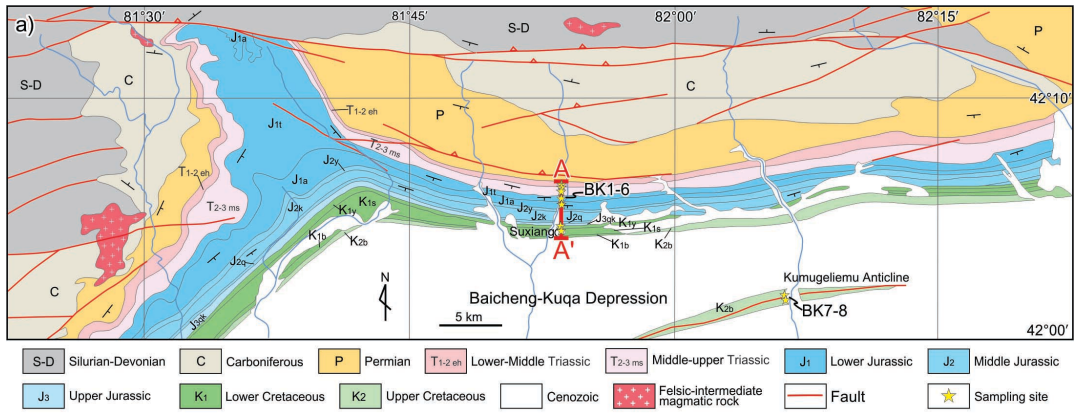

b) Kapushaliang section

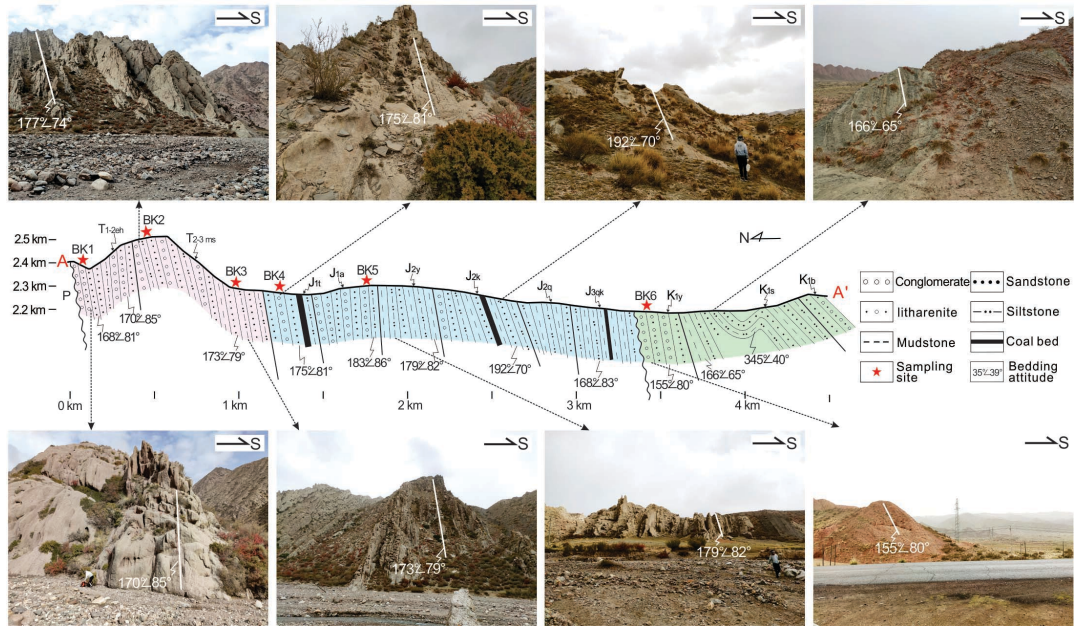

FIGURE 2: (a) Simplified geological map of the study area, AA' is the studied Kapushaliang section. (b) Cross section along the Kapushaliang section based on our field investigations with field images and the sampling sites (red dots) indicated.

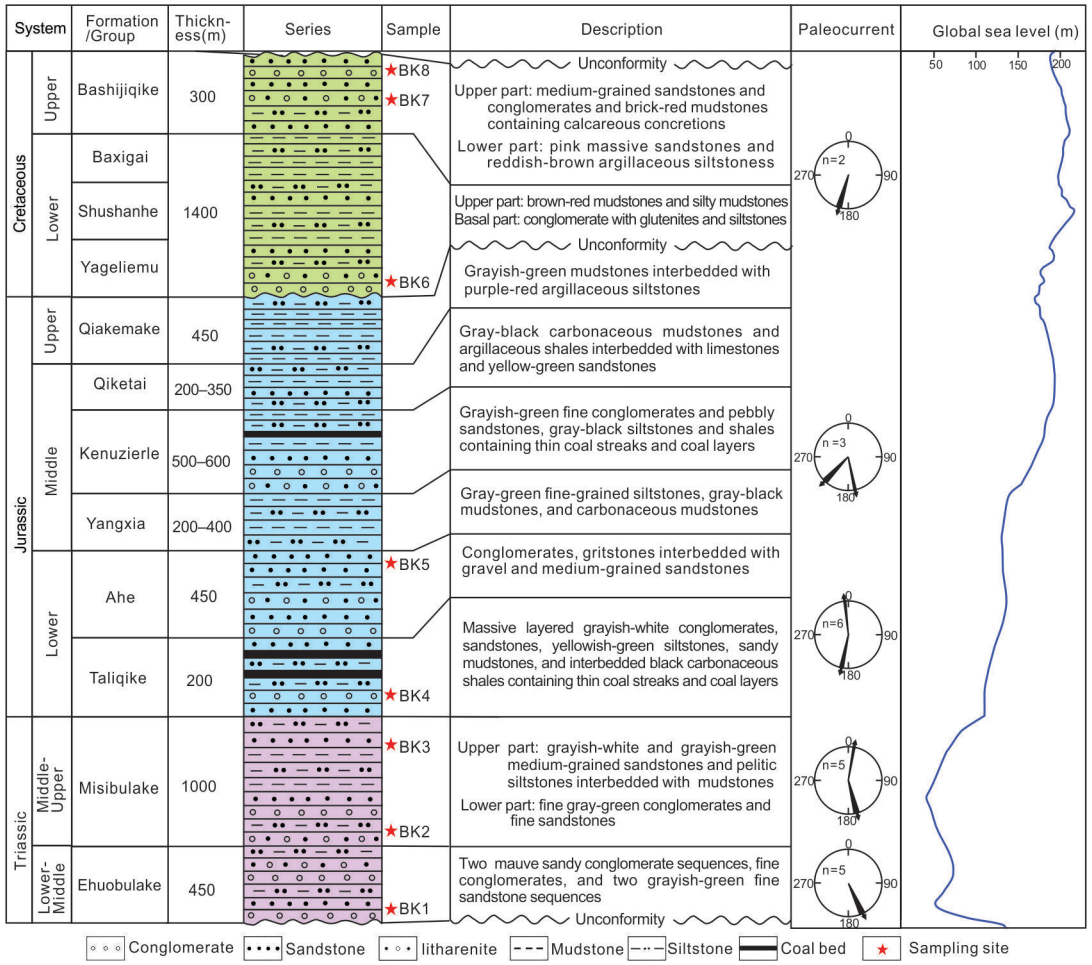

Figure 3: Generalized stratigraphic column and paleocurrent measurements of the Mesozoic succession exposed in the Kapushaliang region. Mesozoic eustatic sea-level curve from Reference 67. Cretaceous marine incursions related to a proto-Paratethys branch occurred in the Tarim basin during a global sea-level rise [68].

3. Sampling and Analytical Methods

3.1. Sampling Strategy. Six sandstone samples were collected through the c. 4.5 km-thick Mesozoic succession exposed along the Kapushaliang section (Figures 2(b) and 3). One sample (BK1) was collected from the Lower-Middle Ehuobulake Group, two samples (BK2, 3) from the Middle-Upper Misibulake Group, one sample (BK4) from the Lower Jurassic Taliqike Formation (Fm.), one sample (BK5) from the Lower Jurassic Ahe Fm., and one sample (BK6) from the Lower Cretaceous Yageliemu Fm (Figure 2). In addition, two samples (BK7, 8) were collected from the Upper Cretaceous Bashijiqike Fm. in the Kumugeliemu Anticline (Figure 2(a)). The Global Position System (GPS) coordinates of each sample are listed in Table 1. Except for sample BK7 (AFT analysis only), detrital AFT analysis, U-Pb age, and trace element concentration were acquired simultaneously during the same ablation for all samples (Supplementary Table S1).

In addition to the analytical data presented in this study, we compiled 1807 published detrital zircon U-Pb ages from twenty-three clastic samples from Mesozoic strata in the Baicheng-Kuqa Depression [7, 11, 22–26] (Supplementary Table S2) in order to further constrain the provenance and paleodrainage reconstruction.

3.2. Apatite U-Pb and Trace Element Analyses. Apatite U-Pb isotopes and trace elements in individual apatite grains were acquired simultaneously from the same ablation using an Agilent 8900 ICP-QQQ coupled to an ESI New Wave NWR 193^{UC} (TwoVol2) laser ablation system at the Beijing Quick-Thermo Science and Technology Co., Ltd. Ablation was carried out for 25 seconds with a 40 μm diameter beam size, c. 3 J/cm^2 energy and 5 Hz repetition rate on the selected grains and reference materials, following Reference 27. Data obtained by LA-QQQ-ICPMS were processed using the Iolite data reduction software [28]. For trace element analysis, ^{43}Ca was used as the internal elemental standard. The primary trace-element reference material employed was NIST SRM 612 standard glass, with Durango apatite used as a secondary trace-element reference material. For U-Pb geochronology, data reduction was undertaken using the VizualAge UcomPbine data reduction scheme of Reference 29, which can account for the presence of variable common-Pb in the primary reference material. Madagascar apatite was used

Table 1: Detrital apatite fission-track data from the Kapushaliang region in the Baicheng-Kuqa Depression (NW China).

Sample	Fm.	Sample location	No. of grains	N_s	ρ_s (N_s) (10^5 cm^{-2})	^{238}U (ppm)	Age range (Ma)	$P(x^2)$%	P1	P2	P3	N_L	MTL (μm ± SE)	Dpar (μm)
Kumugeliemu anticline														
BK8	K_{2b}	N42°1'29.9" E82°6'28.2"	98	11,029	22.70	23.89	98–337	0	139.2 ± 5.1 (24%)	199.5 ± 5.7 (57%)	262 ± 12 (19%)	238	11.49 ± 1.39	1.56
BK7	K_{2b}	N42°1'43.4" E82°6'23.2"	28	940	32.30	41.07	108–326	0	123.3 ± 7.0 (32%)	208 ± 11 (68%)	––	30	11.45±1.46	1.81
Kapushaliang section														
BK6	K_{1y}	N42°4'46.1" E81°53'46.2"	84	5772	16.11	15.21	77–477	0	144.4 ± 5.9 (16%)	199.3 ± 7.3 (31%)	280.9 ± 7.9 (53%)	89	12.22 ± 1.32	1.52
BK5	J_{1a}	N42°5'23.3" E81°53'35.5"	85	5223	13.23	24.40	57–259	0	88.7 ± 4.2 (25%)	120.7 ± 4.4 (64%)	205 ± 18 (11%)	84	12.09 ± 1.91	1.49
BK4	J_{1t}	N42°5'52.6" E81°53'36.2"	94	3244	8.26	24.37	17–269	0	43.6 ± 2.0 (29%)	79.6 ± 2.5 (56%)	172 ± 12 (15%)	42	11.89 ± 2.12	1.46
BK3	$T_{2\text{-}3ms}$	N42°6'6.7" E81°53'53.9″	93	4485	8.13	39.99	18–102	0	34.3 ±0.7 (67%)	70.2 ± 2.3 (33%)	––	79	12.16 ± 2.08	1.68
BK2	$T_{2\text{-}3ms}$	N42°6'19.3" E81°54'1.0″	66	1834	5.32	31.36	19–83	0	29.5 ± 1.7 (67%)	47.1 ± 4.4 (33%)	––	56	12.74 ± 1.83	2.66
BK1	$T_{1\text{-}2eh}$	N42°6'30.6" E81°53'58.4″	53	575	3.47	17.57	18–81	0	27.9 ± 3.0 (32%)	50.8 ± 4.0 (68%)	––	––	––	1.48

N_s, the number of spontaneous fission tracks. ρ_s, spontaneous track density. ^{238}U, uranium content of apatite. P1, P2, and P3 , indicate the ages and modal proportions of the three principal age populations as determined by RadialPlotter.

as the primary age reference material [30], with McClure Mountain [31] used as the secondary age reference material. For single-grain apatite unknowns, we tested the ^{204}Pb- and ^{207}Pb-correction methods, respectively. ^{204}Pb-correction method followed the approach of Reference 32, where the reaction cell between two quadrupoles can allow for online chemical Pb-Hg separation. We ultimately prefer the ^{207}Pb-corrected data in this study as the ^{207}Pb signal is significantly larger than the ^{204}Pb signal. ^{207}Pb-corrected ages were generated using the approach of Reference 33, which iteratively applies a common Pb-correction using the [34] terrestrial Pb evolution model and employing a starting age estimate for each grain. All grains with ^{207}Pb-corrected 2σ age uncertainties of either >25% or >100 Ma were excluded [15].

3.3. AFT Analysis. The AFT method allows for the reconstruction of thermal histories within certain crustal temperature limits. The temperature range of the apatite partial annealing zone (APAZ) is taken as typically ~60°C–110°C [35]. Partial annealing will reduce the apparent AFT age and shorten the lengths of individual tracks, while full annealing will reset the AFT age to zero. The track length distribution constrains the time-temperature path.

AFT analysis was performed at the Institute of Geology and Geophysics, Chinese Academy of Sciences. Apatite grains were embedded in epoxy resin on glass slides, polished to expose internal apatite surfaces, and etched in 5 M HNO_3 at 20°C for 20 seconds to reveal ^{238}U spontaneous fission tracks. Gold coating (c. 5–7 nm thickness) was applied to the etched mounts within a vacuum chamber in order to strengthen the reflectivity of the polished surface and reduce internal reflections under the microscope [36]. Apatite grains with polished surfaces parallel to prismatic crystal faces and homogeneous track distributions were selected and imaged by the Autoscan fission track analysis system which is based on a Zeiss Axio Imager M2m microscope. Fission track density, Dpar measurements, and their orientation with respect to the crystallographic c-axis direction were conducted using the Trackwork and Fasttrack systems [36]. The U concentration of each counted grain was measured by the Laser Ablation Inductively Coupled Plasma Mass Spectrometer (LA-ICP-MS) method following the criteria above. Single-grain AFT ages were calculated using an absolute calibration based on primary constants (aggregate $\xi = 2.001 \times 10^{-3}$). Central ages and the corresponding dispersion of single-grain ages for each sample were calculated and visualized using RadialPlotter [37]. Thermochronological age trends were determined using the criteria summarized in Reference 38.

4. Results and Interpretation

4.1. Detrital Apatite U-Pb and Provenance Interpretation. The magmatic history of the Tianshan orogen, Western Kunlun Orogen, and Pamir area is summarized by the distribution of magmatic ages in Figure 4 and in Supplementary Table S3 to provide a framework for

our provenance analyses. Magmatic rocks in the North Tianshan are mainly restricted to the late Carboniferous to early Permian (Figure 4(b)) [39]. A prominent feature of the Central Tianshan and the Yili Block is the development of widespread and voluminous felsic-intermediate (volcanic and plutonic) magmatism during the Paleozoic, with three pulses at c. 435, 350, and 300 Ma. STS and the northern margin of the Tarim Block were characterized by magmatic quiescence during Late Devonian to Late Carboniferous times (380 and 310 Ma), with two main pulses in magmatic activity from c. 310 to 250 Ma (with a peak at c. 280 Ma) and c. 440 to 400 Ma (with a peak at 420 Ma; Figure 4(b)) [11, 39]. The Western Kunlun Orogen is dominated by Early Paleozoic (c. 540–420 Ma) and Triassic (c. 250–200 Ma) magmatic rocks with only a small cluster between 340 and 320 Ma (Figure 4(b)) [11, 40]. In the Pamir, pulses of magmatism are documented in the Late Cretaceous (with a peak at c. 95 Ma), Eocene (with a peak at c. 40 Ma), Oligocene-Miocene (with peak at c. 15 Ma), and sporadic Late Triassic-Early Jurassic magmatism (with a peak at c. 200 Ma; Figure 4(b); cf. Reference 41).

For convenience, the U-Pb and trace element data from samples BK2 and BK3 (Middle-Upper Triassic Misibulake Group) are plotted together as the provenance information from these two samples is essentially indistinguishable. Similarly, samples BK4 and BK5 (Lower Jurassic strata) are plotted together, as are samples BK6 and BK8 (Cretaceous strata). Of the 702 apatite U-Pb analyses from all samples (BK1–6, BK8) in this study, 511 provided U-Pb ages with acceptable age uncertainties (supplementary Table S1). Adaptive kernel density estimate plots of U-Pb ages [42] and Sr ppm/Y ppm versus light rare earth element (La-Nd) discriminant biplots [16] are provided side-by-side for each sample or sample group in Figure 5. In addition, Tera-Wasserburg Concordia diagrams are presented in Figure S1.

4.1.1. Lower-Middle Triassic Samples. Detrital apatites (sample BK1) in the Lower to Middle Triassic Ehuobulake Group exhibit two major age groups in the Ordovician-Silurian (c. 440–400 Ma) and Late Carboniferous-Permian (c. 325–255 Ma; Figure 5(g) and Figure S1). These two age groups are accompanied by small clusters of Precambrian ages, which are similar to published zircon U-Pb age populations from the Baicheng-Kuqa Depression (Figure 5(g)). The detrital zircon U-Pb literature data are dominated by Paleozoic ages clustering mainly from c. 500–390 Ma and c. 330–260 Ma, with only a few ages between 390 and 330 Ma. The paucity of 390–330 Ma and Triassic U-Pb apatite and zircon ages in the Early-Middle Triassic clastic rocks contrasts strongly with the magmatic record of the CTS-YL regions and Western Kunlun Orogen (Figure 4(b)). Therefore, it is most likely that the material in the Early-Middle Triassic clastic rocks was derived from the northern Tarim and STS regions. This interpretation is in agreement with southeast- or south-directed paleocurrent directions measured in the Lower Triassic sediments (Figures 3 and 6) [12], indicating that the provenance of the Baicheng-Kuqa subbasin is from erosion of the ancestral STS.

4.1.2. Middle-Upper Triassic to Cretaceous Samples. Compared with Lower-Middle Triassic samples, the apatite U-Pb age distributions of Middle-Upper Triassic and Lower Jurassic clastic rocks (samples BK2, 3, 4, and 5) are characterized by a continuous spectrum of Paleozoic and Triassic ages, in particular containing two distinct apatite U-Pb age components at c. 390–330 and 260–220 Ma (Figures 5(c) and 5(e); Figure S1). The 390–330 Ma detrital apatites were probably sourced from the CTS-YL because contemporaneous development of widespread and voluminous felsic-intermediate magmatism is present in this region at this time and is insignificant in the other source regions (Figure 4(b)). However, the c. 260–220 Ma detrital apatites cannot have been derived from the northern Tarim and western Tianshan regions, but a substantial 260–220 Ma magmatic peak is found in the Western Kunlun Orogen (Figure 4(b)). In addition, no dominant paleocurrent direction has been detected in the Kuqa subbasin from the Middle-Late Triassic to the middle Jurassic (Figures 3 and 6) [5, 12], indicating a transition from a single source to multiple sediment sources. Therefore, the Late Triassic to Middle Jurassic sediments deposited in the Baicheng-Kuqa depression were probably sourced from multiple regions, that is, local areas in the northern Tarim and STS, the CTS-YL, NST, and the Western Kunlun Orogen.

The apatite U-Pb age spectra from the Cretaceous clastic rocks are characterized by three main age peaks at c. 460, 400, and 270 Ma (Figure 5(a)). South-directed paleocurrents were documented in Cretaceous strata by sedimentological investigations in the Baicheng-Kuqa depression (Figures 3 and 6) and in the western Tarim Basin of the Pamir-Tianshan corridor [41]. We thus infer that the sediments were most likely sourced from the north, that is, local sourcing from the northern Tarim and STS, CTS-YL, and NST.

4.2. Detrital Apatite Trace Element Compositions. The trace element systematics of detrital apatite, in particular Sr/Y versus light rare earth element (La-Nd) discriminant biplots, are capable of assigning a likely (crystalline) bedrock-source lithology to detrital apatite grains (Figure 5 and associated caption) [16]. The oldest sample in the Lower-Middle Triassic strata contains one hundred and twenty grains. The apatites plot in the Lm (64%), IM (20%), HM (12%), UM (3%), and S (1%) fields in the discrimination diagram (Figure 5(h)).

Detrital apatites in the Middle-Upper Triassic and Lower Jurassic strata show similar trace-element geochemistry and therefore probably reflect a similar provenance (Figures 5(d) and 5(f)). Most grains are derived from mafic and I-type granitoid igneous sources (c. 40%, plotting in the "IM" field) and low-grade metamorphic sources (c. 40%, plotting in the "Lm" field). Some apatites have "HM" (c. 12%), "S" (c. 2%), and "UM" (c. 6%) affinities.

Detrital apatites in the Cretaceous strata show an increase in IM apatite (55%) with a corresponding decrease in Lm apatite (24%). HM-type (15%), UM-type (5%), and S-type (2%) grains form minor populations (Figure 5(b)).

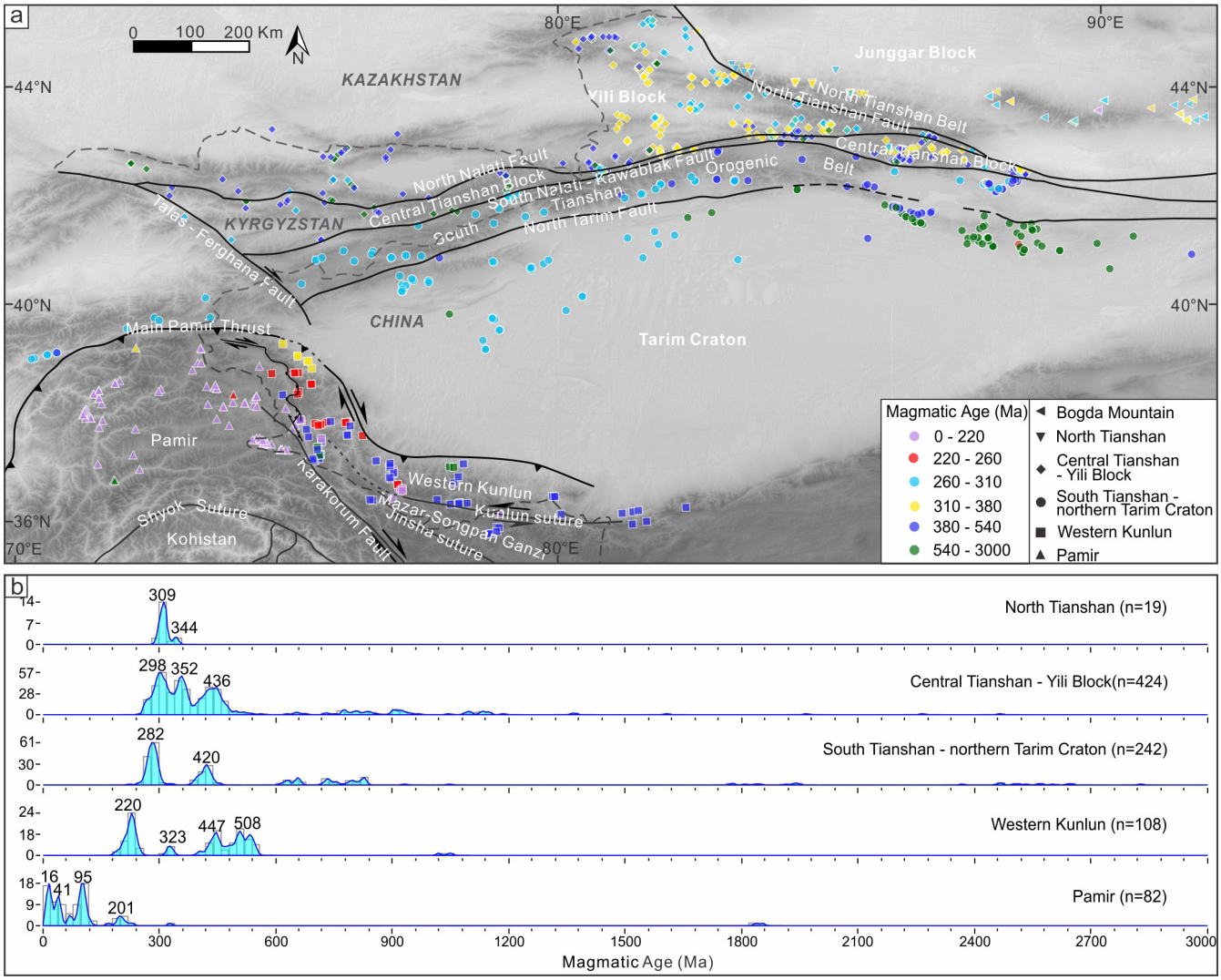

FIGURE 4: (a) Tectonic outline of the Tianshan, Western Kunlun Orogen, and Pamir region, showing ages of igneous/meta-igneous rocks in different tectonic units. Tables of individual ages of units and their associated references can be found in Supplementary Table S3. (b) Age distributions of magmatic units within the Tianshan, Western Kunlun Orogen, and Pamir regions.

4.3. AFT Data. The AFT data display a pattern of younger fission track ages with increasing paleodepth (and thus paleotemperature) that is characteristic of increased annealing at lower structural/stratigraphic levels (Figure 7). All samples exhibit wide dispersion in cooling ages and therefore fail the χ^2 test. Samples BK1–3, 7 are split into two age populations, while the other samples are split into three age groups (Figure 7; Table 1).

The shallowest samples BK7 and BK8 (Cretaceous) have old central AFT ages of 177 ± 11 and 193 ± 5 Ma with single-grain AFT ages ranging from 326 to 108 Ma and from 337 to 98 Ma, respectively. All the single-grain AFT ages are older than the depositional age of c. 80 Ma, indicating that no significant partial annealing has occurred. It is observed that track lengths of basement Mesozoic AFT ages are mostly similar, with the majority yielding lengths of 12–13 μm in the Tianshan range (Figure 8(c)). The cluster of short mean track lengths (MTLs) in the source area indicates an extended residence in the APAZ. However, an MTL of 11.5 μm with a narrow track length distribution (standard deviation <1.5 μm) for samples BK7 and BK8 is slightly shorter than track lengths in the basement source area, implying that post-depositional partial annealing resulted in further minor thermal annealing. Hence, we infer that the exposure to burial temperatures may be c. 60°C–90°C after the tracks formed [35]. These observations suggest that samples BK7 and BK8 were buried by c. 2–3 km (assuming a 22°C/km gradient and mean surface temperature of 20°C [6]) sometime in the middle or late Cenozoic, before being exhumed to the surface.

In the Jurassic-Early Cretaceous samples (samples BK4, BK5, and BK6), the AFT population trends (trends A, B, and C in Figure 9(a)) systematically decrease in age down section, which is compatible with increased annealing structurally/stratigraphically down-section. In the Early Cretaceous sample BK6, the youngest age component approximates the depositional age, whereas the other two

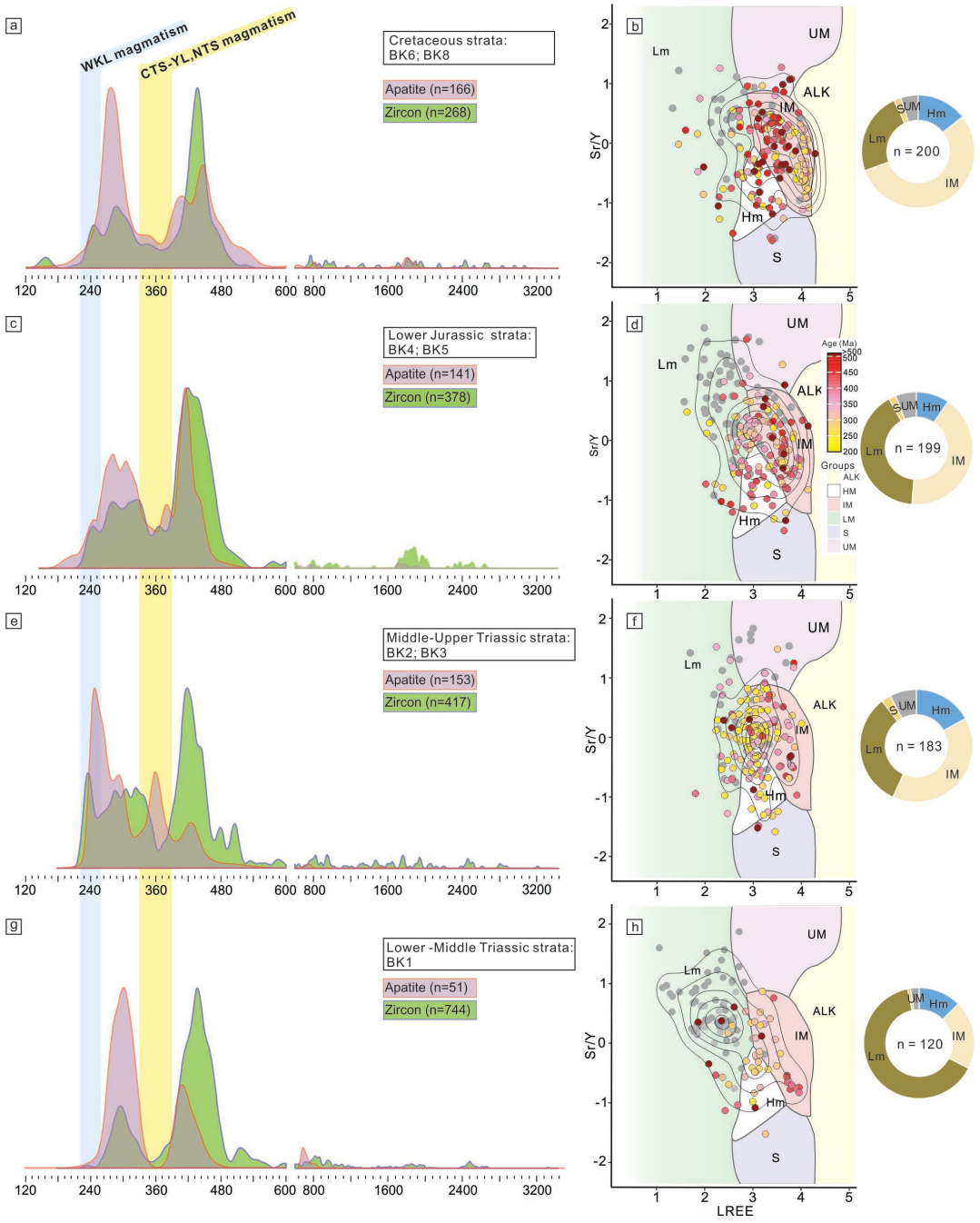

FIGURE 5: Left column: kernel density estimate plots of detrital apatite U-Pb age (pink; see Supplementary Table S1 for data) and detrital zircon U-Pb ages (green; see Supplementary Table S2 for data compilation) in the Baicheng-Kuqa depression. The light yellow band represents magmatic ages (390–330 Ma) characteristic of the Central Tianshan-Yili Block (CTS-YL) and North Tianshan (NTS), whereas the light blue band is magmatic ages (260–220 Ma) characteristic of the Western Kunlun Orogen (WKL; see Figure 4(b)); Right column: apatite Sr/Y versus LREE (ΣLa to Nd) biplots with the lithological discrimination fields of Reference 16 and the proportion of each lithology type for each formation in Kapushaliang region (see Supplementary Table S1 for data). The lithology category acronyms are ALK = alkaline-rich igneous, HM = high-grade metamorphic, IM = I-type granitoids and mafic igneous, LM = low- and medium-grade metamorphic, S = S-type granites, and UM = ultramafic igneous [16]. Grains that provided no U-Pb reliable ages are colored gray on biplots.

age populations are older than the depositional age. The track length distribution is narrow with an MTL of 12.22 ± 1.32 μm, and few tracks are longer than 14 μm. These observations imply partial annealing at maximum burial temperatures of c. 80°C–90°C as burial depth increases, and the apparent sample age becomes younger. For the Lower Jurassic samples BK4 and BK5, most single-grain ages are distinctly younger than the depositional age, yielding MTLs of 11.89 ± 2.12 μm and 12.09 ± 1.91 μm, respectively (Figure 7, Table 1). The track length distribution of

FIGURE 6: Photos showing representative paleocurrent features in the Mesozoic strata of the Kapushaliang region. White arrows indicate paleocurrent orientation. Sedimentary structures in Lower-Middle Triassic, Middle-Late Triassic to Early Jurassic, and Cretaceous strata reveal near-southward, multidirectional paleocurrent, and southward paleocurrents, respectively.

sample BK4 becomes bimodal. The bimodality is due to the combination of a component of early formed tracks that have been strongly shortened by burial heating with a component of long tracks that formed after the heating, which implies that maximum burial temperatures are up to c. 100°C (see path D of Figure 5 in Reference 6).

The three deepest Triassic samples (BK1, 2, and 3) yield single-grain AFT ages that are much younger than the depositional ages, but which are broadly distributed suggesting that these samples have been strongly but not totally annealed. The AFT data exhibit no relationship with the kinetic parameter Dpar and failed the χ^2 test indicating that the data do not comprise a single statistically significant population. We interpret these samples as being strongly but not completely annealed, and these must have been close to, but not hotter than, the lower temperature window

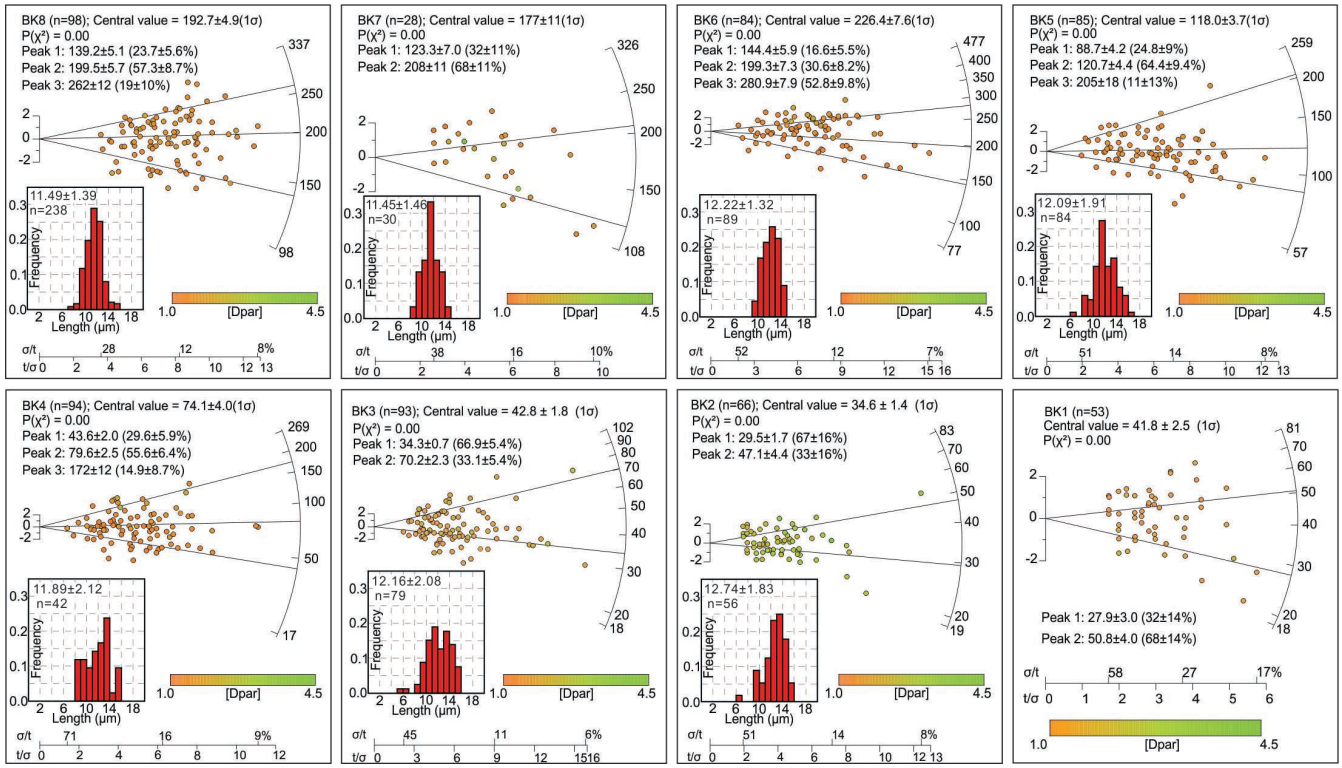

FIGURE 7: Apatite fission track radial plots and corresponding confined track histograms for individual samples from the Kapushaliang region in this study. The single-grain AFT ages are colored according to their Dpar values (in μm).

of the PAZ. Typically, track length distributions from below the break in slope are generally unimodal and have longer MTLs (>14 μm) with smaller standard deviations (<1.5 μm) and reflecting rapid cooling, for example, as shown in the Otway Basin [17]. However, the broadly distributed track lengths (standard deviation >1.8 μm) with many short tracks (MTL <13 μm) also suggest that these samples have not been totally annealed. Samples BK1–3 are interpreted as strongly reset with relatively consistent younger peak ages of c. 30 Ma (Trend A in Figure 9(a)) and older peak ages of 47.1–70.2 Ma (Figure 9(a)). The broadly distributed single-grain ages and track lengths in the three deepest samples indicate that some grains are still not totally annealed (older peaks are still evident in Figure 9(a)), possibly due to the compositional variation between apatite grains, particularly Cl contents. Based on the pronounced but not total annealing of these samples, the single-grain age pattern suggests exposure to temperatures of c. 95°C–125°C (paleodepths of c. 4–5 km) at c. 30 Ma, sufficient to nearly completely reset the single-grain ages at that time (younger peak ages in Figure 9(a)), such that ages of the youngest component grains can be explained as the onset of significant cooling and exhumation at c. 30 Ma (Figure 9).

Thermal history modeling using the software HeFTy (ver. 1.9.1 [43]) was performed on three deeper samples BK2–4 (Figure 10). We use the fact that these samples were at the surface at the age of deposition as the principal constraint in the models, together with a temperature-time box around the AFT ages with temperature intervals ranging from 60°C to 140 °C, a little broader than the typical APAZ. The maximum temperatures reached by the samples, as predicted by the inverse model, increase consistently with increasing paleodepth from ~100°C for BK4, ~115°C for BK3 to ~120°C for BK2. The maximum burial temperature predicted by the thermal modeling also supports the idea that these deepest samples were close to, but not hotter than, the total annealing temperature. The thermal history modeling result for sample BK2 shows a rapid cooling episode commencing at ca. 30 Ma, which is in good agreement with the relatively consistent younger age peaks of the three deepest samples BK1–3. In addition, all samples BK2–4 experienced relatively rapid cooling in the uppermost part of the APAZ from ca. 10 Ma to the present, which indicates Late Miocene cooling. It is supported by previous studies showing that Late Miocene (~10 Ma) rapid exhumation is found across the Tianshan [44–46].

5. Discussion

5.1. Provenance Changes in the Mesozoic Sediments and Implications for the Topographic Evolution of the STS

5.1.1. Early-Middle Triassic Exhumation. The detrital apatite/zircon U-Pb age spectra and south-directed paleocurrents in the Early to Middle Triassic sediments in the Baicheng-Kuqa Depression indicate sourcing from the northern Tarim and STS [11, 24]. The paucity of 390–330 Ma apatite and zircon U-Pb ages indicate the presence of a topographic barrier in STS during the Early to Middle Triassic (Figure 5(g)), which blocked sediment transport

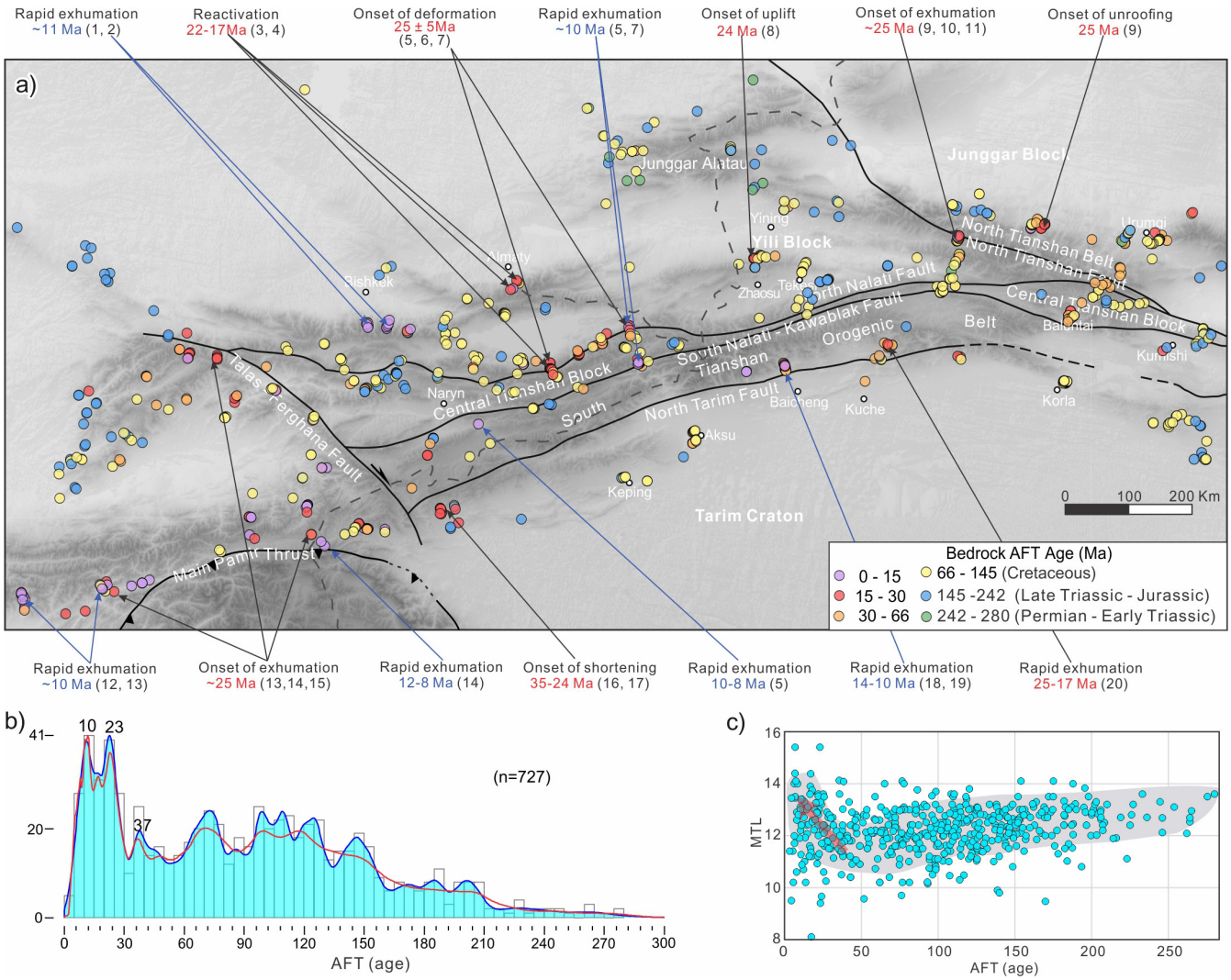

FIGURE 8: (a) Previously published basement AFT ages plotted on a Digital Elevation Model (DEM) of Chinese western Tianshan and Kyrgyz Tianshan (data sources in Supplementary Table S4), with major faults and Cenozoic tectonic events based on AFT data also depicted (1 [44]; 2 [102]; 3 [71]; 4 [70]; 5 [103]; 6 [104]; 7 [105]; 8 [106]; 9 [6]; 10 [107]; 11 [108]; 12 [109]; 13 [110]; 14 [111]; 15 [112]; 16 [113]; 17 [76]; 18 [21]; 19 [45]; 20 [114]). (b) AFT age spectra where blue lines and fill are Kernel density estimate curves, and the red lines are the probability density distribution. (c) "Boomerang plot" of AFT central age against MTL.

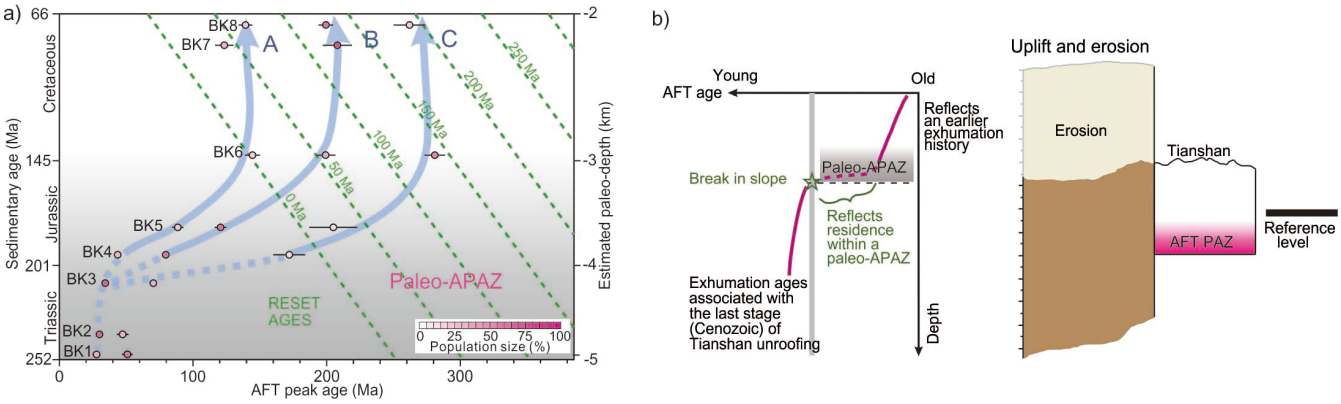

FIGURE 9: (a) Thermochronological age trends through the stratigraphic succession with the white-pink color ramp and letters (A, B, and C) representing the modal percentage of each grain-age population and the moving age peaks discussed in the main text, respectively. Palaeo-depths are estimated based on the extent of AFT annealing and stratigraphic thickness. (b) Schematic diagram showing the expected age trends for the exhumation of a paleo-APAZ and the information that can potentially be retrieved (based on Reference 38).

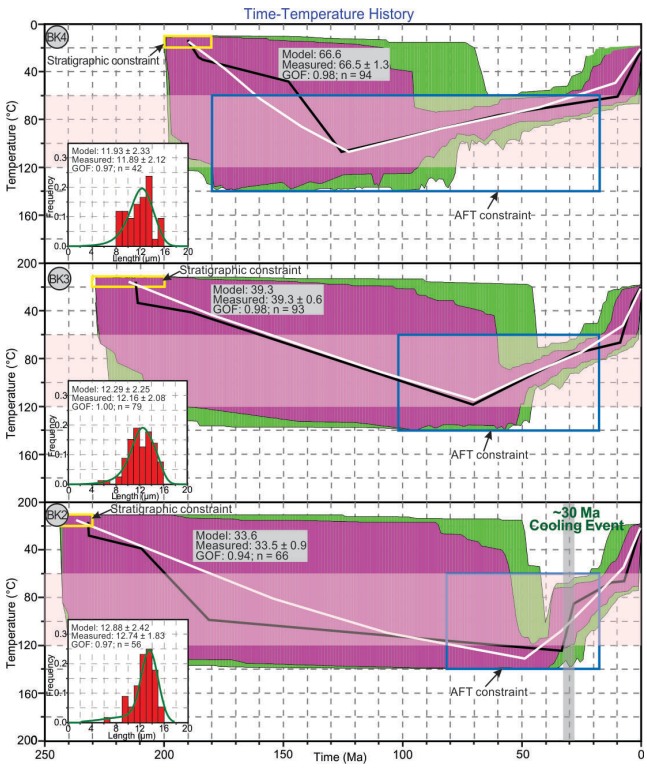

FIGURE 10: Time-temperature history obtained using the HeFTy program [43] for samples BK2-4. Stratigraphic ages (yellow box) were used as the initial constraint in this model, whereas the apatite partial annealing zone and the corresponding AFT ages of the samples were also used as constraints (blue box). Vertical gray-shaded bars highlight the initiation of regional cooling discussed in the text, while horizontal pink zones denote the APAZ. The measured and predicted confined fission track length distribution is presented as an inset. The envelope encompassing all "good" (goodness of fit: GOF > 0.5) paths are colored in purple, and the region encompassing all "acceptable" (GOF > 0.05) paths is colored in green. The black line and white line represent the best-fit path and weighted mean-fit path, respectively, for each model.

from the Yili-Central Tianshan and North Tianshan into the Tarim Basin. Similarly, the Late Carboniferous to Early Triassic sedimentary sequences in the southern margin of the Junggar Basin were almost exclusively derived from the late Palaeozoic magmatic belt of the North Tianshan and the northern margin of the Yili terrane, also indicating a relatively unimodal provenance and development of strong topography in the North Tianshan range [47].

Published Permian to Early Triassic AFT ages for the Tianshan and neighboring regions is limited (Figure 8), likely due to either overprinting by more recent thermotectonic events or subsequent erosion largely removing any low-temperature thermochronological evidence for exhumation at this time. The latest Paleozoic AFT ages were reported at Aksu and along the Dushanzi-Kuqa highway [6] and near the Laerdun Pass (Yili block) [48] in the Tianshan, while Reference 49 obtained Early Permian-Early Triassic AFT ages in the Junggar Alatau on the northern extent of the Tianshan. However, Permian-Triassic titanite fission-track, zircon U-Th/He, and biotite/K-feldspar $^{40}Ar/^{39}Ar$ ages (higher temperature thermochronometers) record the first phase of tectonically induced cooling preserved in the basement of the Tianshan (Figure 11). These cooling ages can be linked to deformation and exhumation in response to the closure of the Palaeo-Asian Ocean [6, 49]. During the Early-Middle Triassic, the STS may have represented the continuation of this Paleozoic orogenic topography, blocking the flow of sediment from the CTS-YL into the Tarim Basin (Figure 12(a)), similar to that hypothesized for the North Tianshan [47].

5.1.2. Middle-Late Triassic to Early Jurassic Regional Tectonic Quiescence and Continuous Peneplanation. A noteworthy feature of the U-Pb age spectra of the Middle-Upper Triassic samples is the appearance of the 390–330 and 260–220 Ma populations (Figure 5), while no dominant paleocurrent direction has been detected in the successions of the Kuqa depression during the Middle-Late Triassic to Middle Jurassic [12]. Combined, these observations imply that the CTS-YL and Western Kunlun Orogen (which have 390–330 and 260–220 Ma magmatic peaks; Figure 4(b)) started to provide detritus to the Baicheng-Kuqa Depression at that time. The STS belt must have been sufficiently denuded to allow sourcing from these neighboring regions into the northern Tarim from the Middle-Late Triassic, implying a decrease in basin-range relief and tectonic subsidence (Figure 12(b)). In addition, a considerable quantity of Triassic igneous plutons had been reported in the East Tianshan region [50–52]. Based on the proximity of the Baicheng-Kuqa Depression to the Western Kunlun Orogen, the absence of a topographic barrier between them, and the widespread and voluminous Triassic magmatic activity in West Kunlun Orogen, the Triassic detritus in the Baicheng-Kuqa Depression was likely mainly derived from the Western Kunlun Orogen, although the Eastern Tianshan may have provided a small amount of distally sourced clastic material.

In the Middle-Late Triassic sedimentary samples, the 390–330 Ma peak is less prominent in the detrital zircon U-Pb spectra than in the detrital apatite U-Pb spectra (Figure 5(e)). Investigating solely the detrital zircon record would lead to the erroneous interpretation that CTS-YL only provided minor detritus to the northern edge of Tarim block. Our detrital apatite U-Pb data disprove this interpretation and show that the CTS-YL started to provide abundant clastic detritus to the northern Tarim Basin at this time.

In the Early Jurassic sedimentary samples, the detrital apatite U-Pb age spectra exhibit strong similarity to the published zircon U-Pb age distributions from the Baicheng-Kuqa Depression [11, 22, 24, 25], with both showing similar 390–330 and 260–220 Ma peaks. In addition, the detrital apatite trace-element geochemistry of the Early Jurassic samples is similar to that of the Middle-Late Triassic samples. There is therefore no obvious change in provenance from the Middle-Late Triassic to Early Jurassic, which implies that subdued topography and/or tectonic subsidence continued in the STS until at least the Early Jurassic times. Moreover, outcrops of Early to

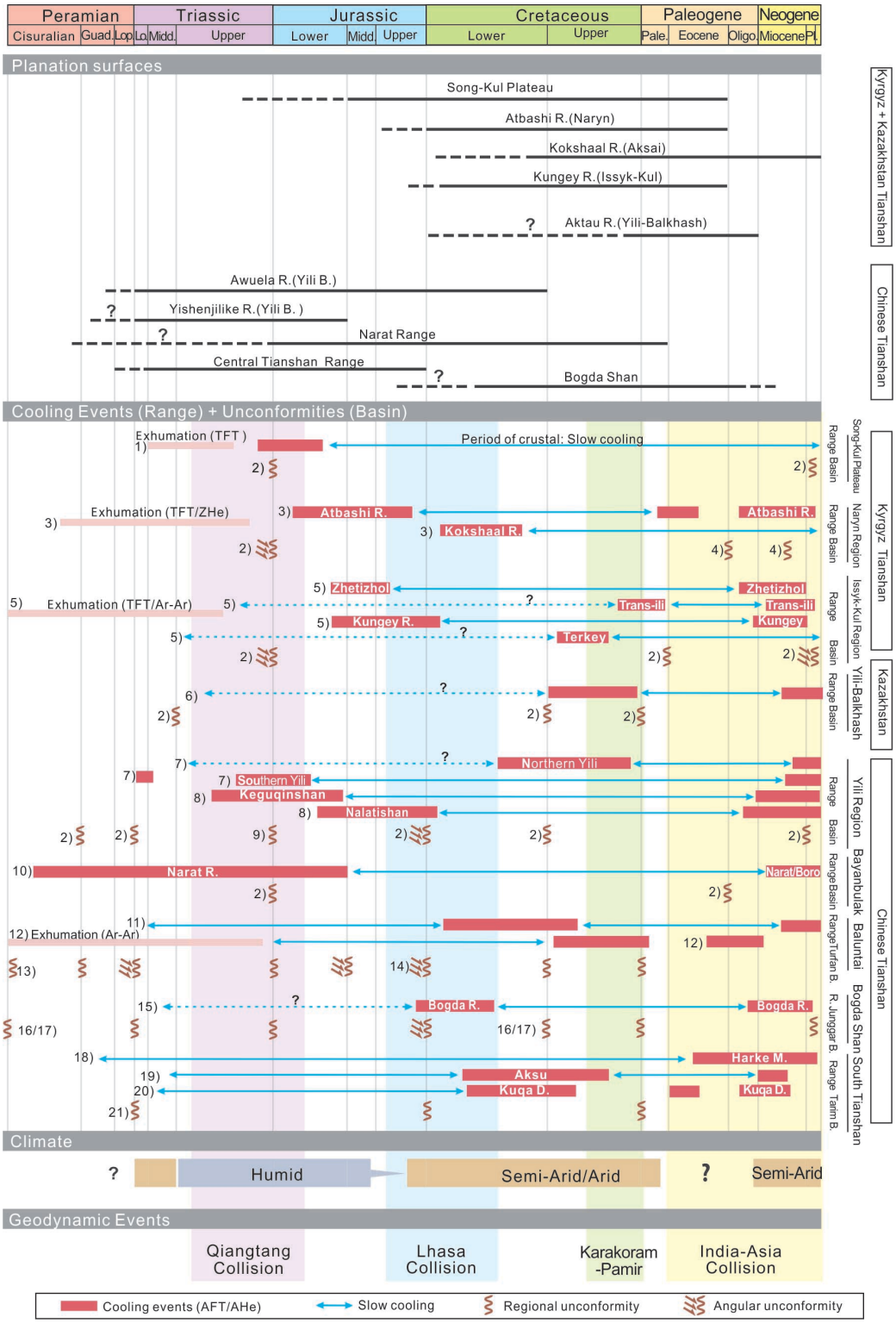

FIGURE 11: Synthesis chart of the Tianshan region compiling available stratigraphic data, low-thermochronology data, ages of the planation surfaces, climate, and geodynamic events (modified from Reference 1; 1 [53]; 2 [1]; 3 [103]; 4 [105]; 5 [71]; 6 [70]; 7 [58]; 8 [115]; 9 [116]; 10 [48]; 11 [54]; 12 [72]; 13 [117]; 14 [118]; 15 [119]; 16 [120]; 17 [5]; 18 [61]; 19 [60]; 20 [6]; 21 [21]).

Middle Jurassic coal-bearing sediments are preserved in the northern/southern piedmonts and interior of the Tianshan, which also suggests low-relief landforms and tectonic quiescence under rather humid conditions in the Chinese Tianshan at that time [22, 24]. The flat erosional surfaces exposed in the Tianshan region were already established during the Late Triassic-Early Jurassic phase of tectonic quiescence, such as the formation of the Song-Kul plateau

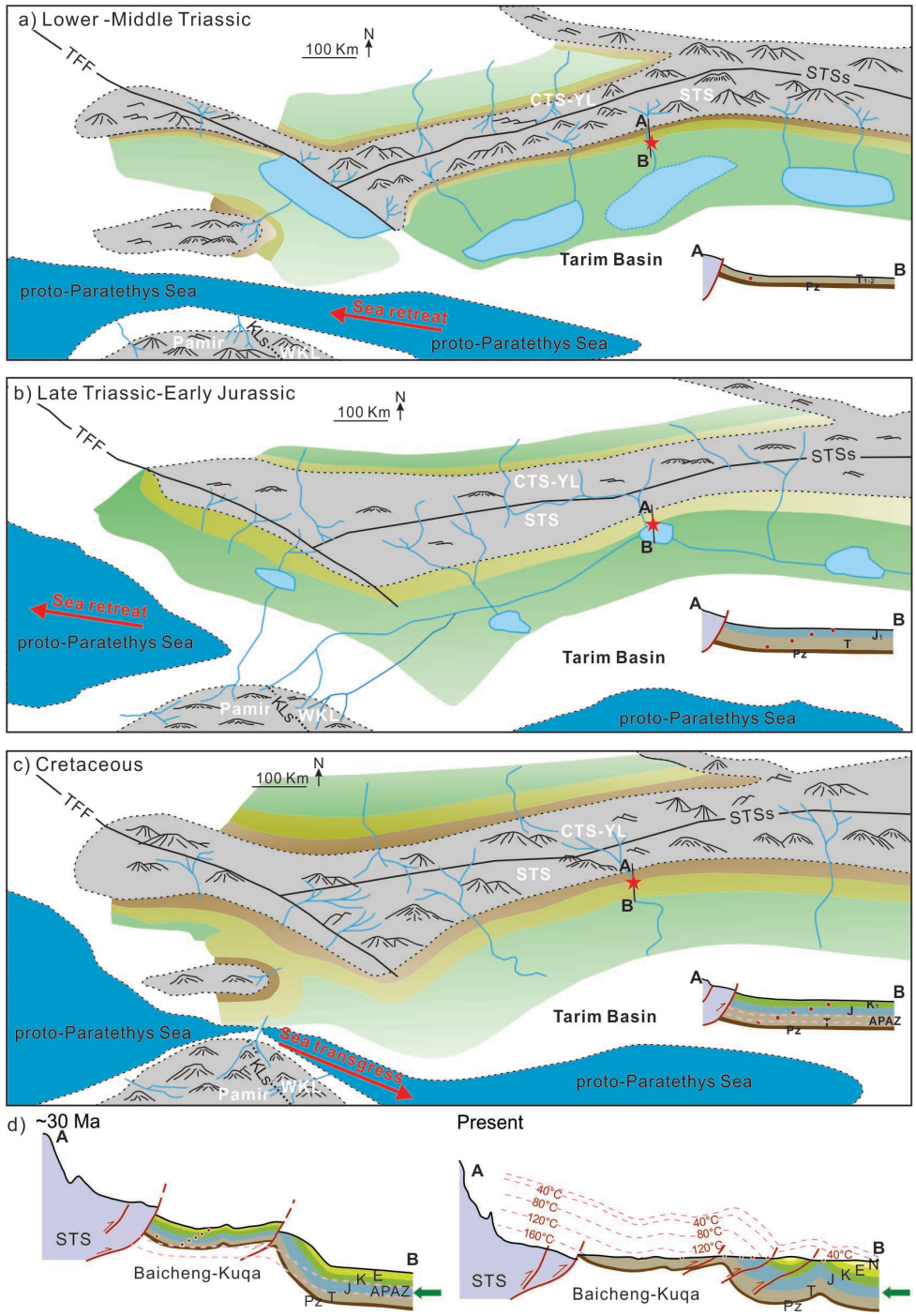

FIGURE 12: (a–c) Paleogeographic reconstructions of the western Tianshan during the Mesozoic (modified after References 55, 56). (d) Structural evolution of the northern margin of the Baicheng-Kuqa depression during Cenozoic as described in the main text. Bold green arrows indicate far-field N-direct shortening propagating from the India-Asia collision. The section is vertically exaggerated. Study sites are denoted by red stars. Gray = site of erosion; brown = alluvial fan environments; yellow = proximal alluvial plain environments; green = distal alluvial plain environments; light blue = lake; dark blue = sea. TFF: Talas-Fergana Fault, STSs: South Tianshan suture, and KLs: Kunlun suture.

morphology in the Middle Jurassic [53], several planation surfaces inside the Chinese Central Tianshan that initiated in the Triassic-Jurassic [54–57], and establishment of planation surfaces within the Narat range during the Triassic-Early Jurassic [1].

Late Triassic-Early Jurassic AFT cooling ages have been obtained from regions with preserved Mesozoic relief (peneplanation surfaces) in northernmost Tianshan [49], the Kyrgyz Tianshan [53], Central Tianshan [54, 58], and the westernmost extent of the Tianshan [59] (Figure 8),

indicating that the old relief preserved a phase of Late Triassic-Early Jurassic enhanced cooling (Figure 11). In addition, this Late Triassic-Early Jurassic tectonic activity and erosion are supported by the presence of an angular unconformity at the base of the Jurassic series within the Issyk-Kul and Naryn basins (Figure 11). These discrete, mostly contractional tectonic events in the Tianshan region have been interpreted as recording accretion of the Qiangtang Block to the Eurasian margin. However, AFT thermochronology studies in Chinese STS show that after the assembly of the Tianshan lithosphere in the Latest Paleozoic, STS was not subjected to uplift until the Cretaceous [6, 60], and hence, the low-relief surfaces/peneplains of Chinese STS could have formed until the onset of unroofing in the Early Cretaceous. Tectonic movement was limited in the Chinese STS during the Early Jurassic to the middle Eocene, with an average exhumation rate of about 0.017 mm/a since the Early Jurassic [61].

Triassic-Early Jurassic cooling has been documented in the southernmost [62], northernmost [63], and foreland basin [64] portions of the West Kunlun Orogen, possibly related to the accretion of the West Kunlun, Songpan-Ganzi, and Tianshuihai terranes [62]. This implies that the West Kunlun ranges were likely exhuming at this time and could therefore supply large amounts of sediments to the active accretionary complex to the south [65], as well as to the Tarim Basin to the north [66]. Furthermore, the global sea level fell substantially during the Triassic (Figure 3) [67], possibly leading to the progressive westward retreat of the proto-Paratethys Sea from the Tarim Basin, allowing detritus to be transported far east of the Tarim Basin into the Baicheng-Kuqa depression without being blocked by the incursion of the proto-Paratethys Sea (Figure 12(b)).

5.1.3. Cretaceous Reactivation. South-directed paleocurrents from the Cretaceous strata in the northern Tarim Basin indicate that the Tianshan Range was the dominant provenance area at this time (Figures 3 and 6) [5, 12]. Furthermore, during the Cretaceous, the proto-Paratethys Sea transgressed into the Fergana, Tarim, Tajik, and Alai basins [55, 68, 69] during a global sea-level rise (Figure 3) [67]. During this time, the eastward transport of sediment from the West Kunlun Orogen to the Baicheng-Kuqa depression was blocked by the incursion of the proto-Paratethys Sea (Figure 12(c)). The detrital apatite and zircon U-Pb age spectra still show minor populations of Triassic material (Figure 5(a)), which may reflect recycling from the underlying Late Triassic-Jurassic succession. While compared with the Middle-Late Triassic and Early Jurassic samples, the 390–330 Ma age population in the Cretaceous samples is significantly smaller, which indicates that sourcing from the CTS-YL was decreasing in importance. Combined, this implies that substantial topography began to develop in the STS in the Early Cretaceous, limiting the flow of sediment from the CTS-YL and North Tianshan into the Tarim Basin (Figure 12(c)).

In contrast to the early Mesozoic cooling event that is only locally preserved within the Tianshan bedrock and in the intramontane Tianshan detrital record, Cretaceous AFT ages are recorded in the entire Tianshan, including across terrane boundaries (Figure 8 and associated references). One possibility for the enhanced cooling rate is the increase of surface erosion triggered by climate change. However, the disappearance of the humid conditions marked by coal layers and the extensive formation of calcareous paleosols reflects increasingly semiarid to acid conditions during the Cretaceous in the Tianshan region, resulting in decreased erosion. Considering that the Cretaceous reactivation and rapid basement cooling were pervasively recorded in the Kazakh [70], Kyrgyz [71], and Chinese Tianshan [6, 48, 60, 72], a tectonic mechanism is more likely to be responsible for the increased cooling rate in the Cretaceous. Tectonic deformation was likely caused by the far-field effects of the Cimmerian Lhasa block collision on the southern Eurasian margin [2, 6] and probably also the contemporaneous Mongol-Okhotsk Orogeny on the eastern Eurasian margin [70, 73].

5.2. Onset of Late Cenozoic Reactivation/Exhumation. Our AFT data show that all the single-grain AFT ages in the Upper Cretaceous samples are older than their depositional ages with MTLs of 11.5 ± 1.4 μm, indicating only slight thermal annealing. Central AFT ages in the Jurassic-Lower Cretaceous succession decrease down-section from 226 to 74 Ma, while corresponding track length distributions broaden down section (standard deviations increase from 1.32 to 2.12 μm) and MTLs decrease (12.22 and 11.89 μm) which reflects increased annealing [35, 74]. The deepest samples (Triassic samples BK1, BK2, and BK3) display the most broadly distributed single-grain ages and track lengths, suggesting that these samples have not been totally annealed. However, the maximum burial temperatures of c. 100°C–120°C predicted by the thermal modeling indicate these deeper samples as being strongly age reset (Figure 10), sufficient to almost completely anneal the single-grain ages, with the youngest peak in Figure 9(a) interpreted as recording exhumation at c. 30 Ma, where they define a break-in-slope in the AFT age-depth plot (Trend A in Figure 9(a)). This may represent the onset of a rapid cooling and unroofing event along the southern margin of the Chinese Tianshan (Figure 12(d)). Rapid cooling at c. 30 Ma is also revealed by our thermal history modeling from sample BK2. This is consistent with previous studies suggesting that Cenozoic uplift and exhumation along the southern front of the Tianshan initiated during late Eocene-Oligocene based on (U-Th)/He data [75], AFT and detrital zircon U/Pb data [76, 77], and magnetostratigraphic data [78]. Similarly, a break in slope observed from the AFT/AHe (apatite [U-Th]/He) age-depth profiles in the southern Junggar Basin implies that rapid cooling/exhumation on the northern margin of the Chinese Tianshan began at c. 25–20 Ma [79, 80]. In addition, the boomerang plot shows a curve back up toward longer MTLs in the Late Palaeogene (red arrow), consistent with the onset of Cenozoic exhumation in the Tianshan (Figure 8(c)).

In addition, Oligocene-early Miocene deformation has been widely reported across the Tibetan Plateau and its margins, for example, at 30–25 Ma along the Longmen

Shan on the eastern margin of the plateau [81], a Late Eocene-Oligocene phase (c. 35–28 Ma) of shortening in the Eastern Tibetan Plateau [82], the onset of faulting along the Southern Qaidam Thrust at c. 35.5 Ma [83], the onset of Cenozoic basin development in the Tibetan Plateau at ca. 30 Ma [84–86], and rapid surface uplift in central Tibet between late Eocene and Oligocene time (ca. 36–25 Ma) based on paleoaltimetry studies [87–89].

There is however growing consensus that Late Miocene (c. 10 Ma) rapid exhumation is widely distributed not only in Tianshan [90–93] (Figures 8(a) and 8(b)) but also in the interior of Tibetan Plateau and its margins [94–97]. Though the causative mechanisms for these two phases (Oligocene-Miocene vs. Late Miocene) remain controversial, the approximate synchronicity between these two phases of accelerated deformation in the Tianshan and the Tibetan Plateau suggests that strain propagated rapidly across the strong Tarim cratonic lithosphere, whereas deformation was focused along the edges of the rigid Tarim block [98]. Although Oligocene-Miocene AFT ages have been widely recognized throughout the Tianshan, regions in the vicinity of large thrust and strike-slip faults (the North Tianshan Fault, the Nalati Fault, Talas-Ferghana Fault, and Main Pamir Thrust) mainly record Late Cenozoic AFT ages. Hence, faults may have played a first-order role in controlling younger (especially Late Cenozoic) exhumation events [54, 99].

6. Conclusions

New apatite U-Pb, fission-track, trace element provenance results, and paleocurrent measurements together with previously published detrital zircon U-Pb and paleocurrent data in the Baicheng-Kuqa depression allow us to reconstruct the Mesozoic tectonic-geomorphic evolution of the STS. Furthermore, the onset of Cenozoic exhumation in Southern Tianshan was constrained by AFT dating on these same samples. The following conclusions have been drawn:

(1) During the Early-Middle Triassic, the STS belt, probably due to inherited topography from Late Paleozoic orogenesis, acted as a barrier to the flow of sediment from the north into the Tarim Basin.

(2) In the Late Triassic to Early Jurassic, the high topography of the STS belt was continuously denuded until it allowed material to be sourced from neighboring regions (Yili-Central Tianshan and Western Kunlun Orogen) into the northern Tarim Basin.

(3) The STS was subjected to Cretaceous reactivation and exhumation and became again the main source for the sediments in the Baicheng-Kuqa depression.

(4) New AFT data reveals that enhanced cooling and exhumation commenced at c. 30 Ma on the southern margin of the Chinese Tianshan. It implies that tectonic deformation related to the India-Asia collision had propagated into the Tianshan at that time. Subsequent (Late Cenozoic) exhumation in the Western Chinese Tianshan is linked to the reactivation of large thrust and strike-slip faults on the northern and southern margins of the Tianshan orogen.

Data Availability

The data for this study are available in this manuscript and supplementary material.

Conflicts of Interest

The authors declare that they have no conflicts of interest.

Acknowledgments

This work was financially supported by NSFC (Grant No. 41888101, 92055213 and 42261144673). David Chew acknowledges support from Science Foundation Ireland (SFI) under Grant Number 13/RC/2092_P2 (iCRAG, the SFI Research Centre in Applied Geosciences).

Supplementary Materials

Figure S1: Tera-Wasserburg diagrams of apatite detritus in the Mesozoic strata of Kapushaliang area, in stratigraphic order. A very small amount of analyses with large error ellipses have been removed for clarity. Supplementary Table S1: Apatite fission track ages, trace elements, and U-Pb isotope information for apatite measured from sedimentary rocks in Kapushaliang area for this study. All data measured by LA-QQQ-ICPMS from the same sampled aliquots. Supplementary Table S2: Compilation of U-Pb data of detrital zircons from Mesozoic sedimentary rocks in the Baicheng-Kuqa depression along the southern flank of the Chinese western Tianshan. Supplementary Table 3: Summary of crystallization ages of magmatic rocks from the West Tianshan Orogen, northern margin of the Tarim Block, Pamir and Western Kunlun Orogen. Supplementary Table S4: Compilation of apatite fission track ages for igneous and bedrock rocks in the Chinese western Tianshan and Kyrgyz Tianshan.

References

[1] J. Morin, M. Jolivet, L. Barrier, A. Laborde, H. Li, and O. Dauteuil, "Planation surfaces of the Tian shan range (central Asia): Insight on several 100 million years of topographic evolution," *Journal of Asian Earth Sciences*, vol. 177, June, pp. 52–65, 2019.

[2] S. Glorie and J. De Grave, "Exhuming the Meso-Cenozoic Kyrgyz Tianshan and Siberian Altai-Sayan: A review based on low-temperature Thermochronology," *Geoscience Frontiers*, vol. 7, no. 2, pp. 155–170, 2016.

[3] W. Xiao, B. F. Windley, S. Sun, et al., "A tale of amalgamation of three Permo-Triassic collage systems in central Asia:

Oroclines, Sutures, and terminal accretion," *Annual Review of Earth and Planetary Sciences*, vol. 43, no. 1, pp. 477–507, 2015. https://www.annualreviews.org/toc/earth/43/1.

[4] W. Xiao, B. F. Windley, C. Han, et al., "Late Paleozoic to early Triassic multiple roll-back and Oroclinal bending of the Mongolia collage in central Asia," *Earth-Science Reviews*, vol. 186, November, pp. 94–128, 2018.

[5] M. S. Hendrix, S. A. Graham, A. R. Carroll, et al., "Sedimentary record and Climatic implications of recurrent deformation in the Tian shan: Evidence from Mesozoic strata of the North Tarim, South Junggar, and Turpan basins, Northwest China," *Geological Society of America Bulletin*, vol. 104, no. 1, pp. 53–79, 1992.

[6] T. A. Dumitru, D. Zhou, E. Z. Chang, et al, "Uplift, Exhumation, and deformation in the Chinese Tian shan," *Geological Society of America Memoir*, vol. 194, pp. 71–99, 2001.

[7] A. R. Carroll, T. A. Dumitru, S. A. Graham, and M. S. Hendrix, "An 800 million-year Detrital Zircon record of Continental amalgamation: Tarim Basin, NW China," *International Geology Review*, vol. 55, no. 7, pp. 818–829, 2013.

[8] C. Jia, G. Wei, B. Li, A. Xiao, and Q. Ran, "Tectonic evolution of two-epoch foreland basins and its control for natural gas accumulation in China′ s mid-Western areas," *Acta Petrolei Sinica*, vol. 24, no. 2, pp. 13–27, 2003.

[9] Z. Guo, C. Wu, Z. Zhang, M. Wang, and S. Fang, "Mesozoic-Cenozoic relationships between Tianshan mountain and peripheral basins: Evidence from sedimentary and Exhumation of Jurassic in Houxia area, Urumchi," *Geological Journal of China Universities*, vol. 11, no. 4, pp. 558–567, 2005.

[10] S. Fang, Z. Guo, C. Wu, Z. Zhang, M. Wang, and Q. Yuan, "Jurassic Clastic composition in the Southern Junggar Basin, Northwest China: Implications for Basin-range pattern and Tectonic attributes," *Acta Geologica Sinica*, vol. 80, no. 2, pp. 196–209, 2006.

[11] Y. Han, G. Zhao, M. Sun, et al., "Detrital Zircon provenance constraints on the initial uplift and Denudation of the Chinese Western Tianshan after the assembly of the Southwestern central Asian Orogenic belt," *Sedimentary Geology*, vol. 339, June, pp. 1–12, 2016.

[12] Z. Li, W. J. Song, S. T. Peng, D. X. Wang, and Z. P. Zhang, "Mesozoic-Cenozoic Tectonic relationships between the Kuqa Subbasin and Tian shan, Northwest China: Constraints from Depositional records," *Sedimentary Geology*, vol. 172, nos. 3–4, pp. 223–249, 2004.

[13] R. O. Lease, D. W. Burbank, B. Hough, Z. C. Wang, and D. Y. Yuan, "Pulsed Miocene range growth in northeastern Tibet: Insights from Xunhua Basin Magnetostratigraphy and provenance," *Geological Society of America Bulletin*, vol. 124, nos. 5–6, pp. 657–677, 2012.

[14] D. E. Barber, D. F. Stockli, and F. Galster, "The Proto-Zagros foreland basin in Lorestan, Western Iran: Insights from Multimineral Detrital Geothermochronometric and trace elemental provenance analysis," *Geochemistry, Geophysics, Geosystems*, vol. 20, no. 6, pp. 2657–2680, 2019.

[15] D. Chew, G. O'Sullivan, L. Caracciolo, C. Mark, and S. Tyrrell, "Sourcing the sand: Accessory mineral fertility, Analytical and other biases in Detrital U-PB provenance analysis," *Earth-Science Reviews*, vol. 202, March, p. 103093, 2020.

[16] G. O'Sullivan, D. Chew, G. Kenny, I. Henrichs, and D. Mulligan, "The trace element composition of Apatite and its application to Detrital provenance studies," *Earth-Science Reviews*, vol. 201, February, p. 103044, 2020.

[17] M. G. Malusà and P. G. Fitzgerald, *Fission-Track Thermochronology and Its Application to Geology,* Springer International Publishing, Cham, Switzerland, 2019. http://link.springer.com/10.1007/978-3-319-89421-8.

[18] B. Wang, D. Cluzel, L. Shu, et al., "Evolution of Calc-alkaline to alkaline Magmatism through Carboniferous convergence to Permian Transcurrent Tectonics, Western Chinese Tianshan," *International Journal of Earth Sciences*, vol. 98, no. 6, pp. 1275–1298, 2009.

[19] D. V. Alexeiev, Y. S. Biske, B. Wang, et al., "Tectono-Stratigraphic framework and Palaeozoic evolution of the Chinese South Tianshan," *Geotectonics*, vol. 49, no. 2, pp. 93–122, 2015.

[20] Geological and Mineral Resources Bureau of Xinjiang Uygur Autonomous Region, Regional Geology of Xinjiang Uygur Autonomous Region, Ministry of Geology and Mineral Resources of the People's Republic of China, *Geological Memoirs*, 1993.

[21] W. Yang, J. Li, Z. Guo, M. Jolivet, and G. Heilbronn, "New Apatite fission-track ages of the Western Kuqa depression: Implications for the Mesozoic-Cenozoic Tectonic evolution of South Tianshan, Xinjiang," *Acta Geologica Sinica*, vol. 91, no. 2, pp. 396–413, 2017. http://doi.wiley.com/10.1111/acgs.2017.91.issue-2.

[22] M. Wang, J. J. Zhang, and K. Liu, "Continuous Denudation and Pediplanation of the Chinese Western Tianshan Orogen during Triassic to middle Jurassic: Integrated evidence from Detrital Zircon age and heavy mineral chemical data," *Journal of Asian Earth Sciences*, vol. 113, December, pp. 310–324, 2015.

[23] Z. Li and S. T. Peng, "Detrital Zircon Geochronology and its provenance implications: Responses to Jurassic through Neogene Basin-range interactions along northern margin of the Tarim Basin, Northwest China," *Basin Research*, vol. 22, no. 1, pp. 126–138, 2010. http://blackwell-synergy.com/doi/abs/10.1111/bre.2010.22.issue-1.

[24] D. Liu, M. Jolivet, W. Yang, et al., "Latest Paleozoic-early Mesozoic Basin-range interactions in South Tian shan (Northwest China) and their Tectonic significance: Constraints from Detrital Zircon U-PB ages," *Tectonophysics*, vol. 599, June, pp. 197–213, 2013.

[25] H. Huang, Z. Zhang, M. Santosh, Z. Cheng, T. Wang, and Y. Liu, "Crustal evolution in the South Tianshan Terrane: Constraints from Detrital Zircon Geochronology and implications for Continental growth in the central Asian Orogenic belt," *Geological Journal*, vol. 54, no. 3, pp. 1379–1400, 2019. https://onlinelibrary.wiley.com/toc/10991034/54/3.

[26] J. Chang, Y. Zhang, N. Qiu, and C. Li, "Uplift and Exhumation in the Tianshan, Western China: New insights from Detrital Zircon morphology and Thermochronology," *Science China Earth Sciences*, vol. 65, no. 3, pp. 449–461, 2022.

[27] Z. Zhang, T. Zack, B. Kohn, et al., "From Tethyan Subduction to Arabia-Eurasia Continental collision: Multiple Geo-Thermochronological signals from Granitoids in NW Iran,"

Palaeogeography, Palaeoclimatology, Palaeoecology, vol. 621, July, 2023.

[28] C. Paton, J. Hellstrom, B. Paul, J. Woodhead, and J. Hergt, "Iolite: Freeware for the Visualisation and processing of mass spectrometric data," *Journal of Analytical Atomic Spectrometry*, vol. 26, no. 12, 2011.

[29] D. M. Chew, J. A. Petrus, and B. S. Kamber, "U-PB LA-ICPMS dating using accessory mineral standards with variable common PB," *Chemical Geology*, vol. 363, January, pp. 185–199, 2014.

[30] S. N. Thomson, G. E. Gehrels, J. Ruiz, and R. Buchwaldt, "Routine low-damage Apatite U-PB dating using laser ablation-Multicollector-ICPMS," *Geochemistry, Geophysics, Geosystems*, vol. 13, no. 2, 2012.

[31] B. Schoene and S. A. Bowring, "U–PB SYSTEMATICS of the McClure mountain Syenite: Thermochronological constraints on the age of the $^{40}Ar/^{39}Ar$ standard Mmhb," *Contributions to Mineralogy and Petrology*, vol. 151, no. 5, pp. 615–630, 2006.

[32] D. Xiang, Z. Zhang, T. Zack, et al., "Apatite U-PB dating with common PB correction using LA-ICP-MS/MS," *Geostandards and Geoanalytical Research*, vol. 45, no. 4, pp. 621–642, 2021. https://onlinelibrary.wiley.com/toc/1751908x/45/4.

[33] D. M. Chew, P. J. Sylvester, and M. N. Tubrett, "U-PB and th-PB dating of Apatite by LA-ICPMS," *Chemical Geology*, vol. 280, nos. 1–2, pp. 200–216, 2011.

[34] J. S. Stacey and J. D. Kramers, "Approximation of terrestrial lead Isotope evolution by a two-stage model," *Earth and Planetary Science Letters*, vol. 26, no. 2, pp. 207–221, 1975.

[35] P. F. Green, I. R. Duddy, G. M. Laslett, K. A. Hegarty, A. J. W. Gleadow, and J. F. Lovering, "Thermal Annealing of fission tracks in Apatite 4. quantitative Modelling techniques and extension to geological Timescales," *Chemical Geology*, vol. 79, no. 2, pp. 155–182, 1989.

[36] A. J. W. Gleadow, S. J. Gleadow, D. X. Belton, B. P. Kohn, M. S. Krochmal, and R. W. Brown, "Coincidence mapping-a key strategy for the automatic counting of fission tracks in natural minerals," *Geological Society, London, Special Publications*, vol. 324, no. 1, pp. 25–36, 2009.

[37] P. Vermeesch, "Radialplotter: A Java application for fission track, luminescence and other radial plots," *Radiation Measurements*, vol. 44, no. 4, pp. 409–410, 2009.

[38] M. G. Malusà and P. G. Fitzgerald, "The geologic interpretation of the Detrital Thermochronology record within a Stratigraphic framework, with examples from the European Alps, Taiwan and the Himalayas," *Earth-Science Reviews*, vol. 201, February, p. 103074, 2020.

[39] M. Wang, B. Zhang, R. Ren, et al., "Tracing Tectonic processes from Oceanic Subduction to Continental collision through Detrital Zircon U-PB and LU-HF Isotope data: An example from the Chinese West Tianshan Orogen," *Gondwana Research*, vol. 105, May, pp. 185–200, 2022.

[40] C. Wang, L. Liu, W. Yang, Y. Cao, and R. H. Smithies, "Mafic Magma-driven Magmatic processes and compositional variation in Granitic Pluton construction: The Buya intrusion of West Kunlun, Northwestern China," *Geosphere*, vol. 18, no. 4, pp. 1247–1263, 2022.

[41] Y. Jia, C. Glotzbach, L. Lü, and T. A. Ehlers, "Cenozoic Tectono-Geomorphologic evolution of the Pamir-Tian shan convergence zone: Evidence from Detrital Zircon U-Pb provenance analyses," *Tectonics*, vol. 40, no. 10, 2021.

[42] P. Vermeesch, "On the Visualisation of Detrital age distributions," *Chemical Geology*, vols. 312–313, June, pp. 190–194, 2012.

[43] R. A. Ketcham, "Forward and inverse modeling of low-temperature Thermochronometry data," *Reviews in Mineralogy and Geochemistry*, vol. 58, no. 1, pp. 275–314, 2005.

[44] M. E. Bullen, D. W. Burbank, and J. I. Garver, "Building the northern Tien shan: Integrated thermal, structural, and topographic constraints," *The Journal of Geology*, vol. 111, no. 2, pp. 149–165, 2003.

[45] J. Chang, S. Glorie, N. Qiu, K. Min, Y. Xiao, and W. Xu, "Late Miocene (10.0~6.0 ma) rapid Exhumation of the Chinese South Tianshan: Implications for the timing of Aridification in the Tarim Basin," *Geophysical Research Letters*, vol. 48, no. 3, 2021.

[46] J. Charreau, S. Gilder, Y. Chen, et al., "Magnetostratigraphy of the Yaha section, Tarim Basin (China): 11 ma acceleration in erosion and uplift of the Tian shan mountains," *Geology*, vol. 34, no. 3, 2006.

[47] W. Yang, M. Jolivet, G. Dupont-Nivet, Z. Guo, Z. Zhang, and C. Wu, "Source to sink relations between the Tian shan and Junggar Basin (Northwest China) from late Palaeozoic to Quaternary: Evidence from Detrital U-Pb Zircon Geochronology," *Basin Research*, vol. 25, no. 2, pp. 219–240, 2013.

[48] M. Jolivet, S. Dominguez, J. Charreau, Y. Chen, Y. Li, and Q. Wang, "Mesozoic and Cenozoic Tectonic history of the central Chinese Tian shan: Reactivated Tectonic structures and active deformation," *Tectonics*, vol. 29, no. 6, 2010.

[49] S. Glorie, A. Otasevic, J. Gillespie, et al., "Thermo-Tectonic history of the Junggar Alatau within the central Asian Orogenic belt (SE Kazakhstan, NW China): Insights from integrated Apatite U/PB, fission track and (U–Th)/He Thermochronology," *Geoscience Frontiers*, vol. 10, no. 6, pp. 2153–2166, 2019.

[50] Q. Mao, S. Ao, B. F. Windley, J. Wang, Y. Li, and W. Xiao, "Middle Triassic lower Crust-Derived Adakitic Magmatism: Thickening of the Dananhu Intra-Oceanic arc and its implications for arc–arc amalgamation in the Eastern Tianshan (NW China)," *Geological Journal*, vol. 56, no. 6, pp. 3137–3154, 2021. https://onlinelibrary.wiley.com/toc/10991034/56/6.

[51] K. Wang, W. Xiao, B. F. Windley, et al., "The Dashui Subduction complex in the Eastern Tianshan-Beishan Orogen (NW China): Long-lasting Subduction-accretion terminated by unique mid-Triassic strike-slip juxtaposition of arcs in the Southern Altaids," *Tectonics*, vol. 41, no. 6, p. e2021TC007190, 2022.

[52] Z. Tan, W. Xiao, Q. Mao, et al., "Final closure of the paleo Asian ocean basin in the early Triassic," *Communications Earth & Environment*, vol. 3, no. 1, p. 259, 2022.

[53] J. De Grave, S. Glorie, M. M. Buslov, et al., "The Thermo-Tectonic history of the song-Kul plateau, Kyrgyz Tien shan: Constraints by Apatite and Titanite Thermochronometry and Zircon U/PB dating," *Gondwana Research*, vol. 20, no. 4, pp. 745–763, 2011.

[54] Z. He, B. Wang, S. Nachtergaele, et al., "Long-term topographic evolution of the central Tianshan (NW China)

constrained by low-temperature Thermochronology," *Tectonophysics*, vol. 817, October, p. 229066, 2021.

[55] E. De Pelsmaeker, M. Jolivet, A. Laborde, et al., "Source-to-sink Dynamics in the Kyrgyz Tien shan from the Jurassic to the Paleogene: Insights from Sedimentological and Detrital Zircon U-PB analyses," *Gondwana Research*, vol. 54, February, pp. 180–204, 2018.

[56] J. Morin, M. Jolivet, C. Robin, et al., "Jurassic Paleogeography of the Tian shan: An evolution driven by far-field Tectonics and climate," *Earth-Science Reviews*, vol. 187, December, pp. 286–313, 2018.

[57] M. Jolivet, "Mesozoic Tectonic and topographic evolution of central Asia and Tibet: A preliminary synthesis," *Geological Society, London, Special Publications*, vol. 427, no. 1, pp. 19–55, 2017.

[58] Z. He, B. Wang, W. Su, et al., "Meso-Cenozoic Thermo-Tectonic evolution of the Yili block within the central Asian Orogenic belt (NW China): Insights from Apatite fission track Thermochronology," *Tectonophysics*, vol. 823, January, p. 229194, 2022.

[59] G. Jepson, S. Glorie, A. K. Khudoley, et al., "The Mesozoic Exhumation history of the Karatau-Talas range, Western Tian shan, Kazakhstan-Kyrgyzstan," *Tectonophysics*, vol. 814, September, p. 228977, 2021.

[60] Z. Zhang, W. Zhu, L. Shu, et al., "Apatite fission track Thermochronology of the Precambrian Aksu Blueschist, NW China: Implications for Thermo-Tectonic evolution of the North Tarim basement," *Gondwana Research*, vol. 16, no. 2, pp. 182–188, 2009.

[61] B. Zhang, W. Chen, J. Sun, et al., "The thermal history and uplift process of the Ouxidaban Pluton in the South Tianshan Orogen: Evidence from Ar-Ar and (U-Th)/He," *Science China Earth Sciences*, vol. 59, no. 2, pp. 349–361, 2016.

[62] G. Li, M. Sandiford, A. Fang, et al., "Multi-stage Exhumation history of the West Kunlun Orogen and the amalgamation of the Tibetan plateau," *Earth and Planetary Science Letters*, vol. 528, December, p. 115833, 2019.

[63] E. Cowgill, "Tectonic evolution of the Altyn Tagh-Western Kunlun fault system, Northwestern China," , [Doctoral dissertation], University of California, Los Angeles, 2001.

[64] K. Cao, G.-C. Wang, M. Bernet, P. van der Beek, and K.-X. Zhang, "Exhumation history of the West Kunlun mountains, Northwestern Tibet: Evidence for a long-lived, Rejuvenated Orogen," *Earth and Planetary Science Letters*, vol. 432, December, pp. 391–403, 2015.

[65] L. Ding, D. Yang, F. L. Cai, et al., "Provenance analysis of the Meso-Zoic Hoh-Xil-Songpan-Ganzi Turbidites in northern Tibet: Implications for the Tectonic evolution of the Eastern paleo-Tethys ocean," *Tectonics*, vol. 32, no. 1, pp. 34–48, 2013. http://doi.wiley.com/10.1002/tect.v32.1.

[66] C. Z. Jia, S. B. Zhang, and S. Z. Wu, *Stratigraphy of the Tarim Basin and Adjacent Areas*, Science Press, Beijing, 2004.

[67] D. G. van der Meer, C. R. Scotese, B. J. W. Mills, A. Sluijs, A.-P. van den Berg van Saparoea, and R. M. B. van de Weg, "Long-term Phanerozoic global mean sea level: Insights from Strontium Isotope variations and estimates of Continental Glaciation," *Gondwana Research*, vol. 111, November, pp. 103–121, 2022.

[68] R. Bosboom, G. Dupont-Nivet, A. Grothe, et al., "Timing, cause and impact of the late Eocene stepwise sea retreat from the Tarim Basin (West China)," *Palaeogeography, Palaeoclimatology, Palaeoecology*, vol. 403, June, pp. 101–118, 2014.

[69] J. Sun, J. Sha, B. F. Windley, Z. Zhang, and B. Fu, "Late Eocene stepwise seawater retreat from the Pamir-Tian shan convergence zone (Alay valley) in the Western Tarim Basin, China," *Palaeogeography, Palaeoclimatology, Palaeoecology*, vol. 622, July, p. 111603, 2023.

[70] E. De Pelsmaeker, S. Glorie, M. M. Buslov, et al., "Late-Paleozoic Emplacement and Meso-Cenozoic reactivation of the Southern Kazakhstan Granitoid basement," *Tectonophysics*, vol. 662, November, pp. 416–433, 2015.

[71] J. De Grave, S. Glorie, M. M. Buslov, et al., "Thermo-Tectonic history of the Issyk-Kul basement (Kyrgyz northern Tien shan, central Asia)," *Gondwana Research*, vol. 23, no. 3, pp. 998–1020, 2013.

[72] B. Zhang, W. Chen, J. Liu, J. Yin, and J. Sun, "Thermochronological insights into the Intracontinental Orogeny of the Chinese Western Tianshan Orogen," *Journal of Asian Earth Sciences*, vol. 194, June, p. 103927, 2020.

[73] M. Jolivet, T. De Boisgrollier, C. Petit, et al., "How old is the Baikal rift zone? insight from Apatite fission track Thermochronology," *Tectonics*, vol. 28, no. 3, p. n, 2009.

[74] A. J. W. Gleadow, I. R. Duddy, and J. F. Lovering, "Fission track analysis: A new tool for the evaluation of thermal histories and hydrocarbon potential," *The APPEA Journal*, vol. 23, no. 1, p. 93, 1983.

[75] S. Yu, W. Chen, N. J. Evans, et al., "Cenozoic uplift, Exhumation and deformation in the North Kuqa depression, China as constrained by (U–Th)/He Thermochronometry," *Tectonophysics*, vol. 630, September, pp. 166–182, 2014.

[76] Y. Y. Jia, B. H. Fu, M. Jolivet, and S. Zheng, "Cenozoic Tectono-Geomorphological growth of the SW Chinese Tian shan: Insight from AFT and Detrital Zircon U-PB data," *Journal of Asian Earth Sciences*, vol. 111, November, pp. 395–413, 2015.

[77] W. Yang, M. Jolivet, G. Dupont-Nivet, and Z. Guo, "Mesozoic – Cenozoic Tectonic evolution of Southwestern Tian shan: Evidence from Detrital Zircon U/PB and Apatite fission track ages of the Ulugqat area, Northwest China," *Gondwana Research*, vol. 26, nos. 3–4, pp. 986–1008, 2014.

[78] T. Zhang, X. Fang, C. Song, E. Appel, and Y. Wang, "Cenozoic Tectonic deformation and uplift of the South Tian shan: Implications from Magnetostratigraphy and balanced cross-section restoration of the Kuqa depression," *Tectonophysics*, vol. 628, July, pp. 172–187, 2014.

[79] M. S. Hendrix, T. A. Dumitru, and S. A. Graham, "Late Oligocene-early Miocene Unroofing in the Chinese Tien shan: An early effect of the India-Asia collision," *Geology*, vol. 22, no. 6, p. 487, 1994.

[80] J. Yu, D. Zheng, H. Zhang, et al., "Initial Cenozoic Exhumation of the northern Chinese Tian shan deduced from Apatite (U-Th)/He Thermochronological data," *Lithosphere*, vol. 2022, no. 1, 2022.

[81] E. Wang, E. Kirby, K. P. Furlong, et al., "Two-phase growth of high topography in Eastern Tibet during the Cenozoic," *Nature Geoscience*, vol. 5, no. 9, pp. 640–645, 2012.

[82] Y. Tian, B. P. Kohn, N. Qiu, et al., "Eocene to Miocene out-of-sequence deformation in the Eastern Tibetan plateau: Insights from shortening structures in the Sichuan Basin,"

Journal of Geophysical Research, vol. 123, no. 2, pp. 1840–1855, 2018. http://doi.wiley.com/10.1002/jgrb.v123.2.

[83] F. Cheng, C. Garzione, M. Jolivet, Z. Guo, D. Zhang, and C. Zhang, "A new sediment accumulation model of Cenozoic Depositional ages from the Qaidam Basin, Tibetan plateau," *Journal of Geophysical Research*, vol. 123, no. 11, pp. 3101–3121, 2018.

[84] X. Fang, C. Garzione, R. Van der Voo, J. Li, and M. Fan, "Flexural subsidence by 29 ma on the NE edge of Tibet from the Magnetostratigraphy of Linxia Basin, China," *Earth and Planetary Science Letters*, vol. 210, nos. 3–4, pp. 545–560, 2003.

[85] W. Wang, W. Zheng, P. Zhang, et al., "Expansion of the Tibetan plateau during the Neogene," *Nature Communications*, vol. 8, 2017.

[86] R. Zhou, J. C. Aitchison, K. Lokho, E. R. Sobel, Y. Feng, and J. Zhao, "Unroofing the Ladakh Batholith: Constraints from autochthonous Molasse of the Indus Basin, NW Himalaya," *Journal of the Geological Society*, vol. 177, no. 4, pp. 818–825, 2020.

[87] D. B. Rowley and B. S. Currie, "Currie, Palaeo-Altimetry of the late Eocene to Miocene Lunpola Basin, central Tibet," *Nature*, vol. 439, no. 7077, pp. 677–681, 2006.

[88] P. G. DeCelles, J. Quade, P. Kapp, M. Fan, D. L. Dettman, and L. Ding, "High and dry in central Tibet during the late Oligocene," *Earth and Planetary Science Letters*, vol. 253, nos. 3–4, pp. 389–401, 2007.

[89] Y. Wei, K. Zhang, C. N. Garzione, Y. Xu, B. Song, and J. Ji, "Low Palaeoelevation of the northern Lhasa Terrane during late Eocene: Fossil Foraminifera and stable Isotope evidence from the Gerze Basin," *Scientific Reports*, vol. 6, no. 1, p. 27508, 2016.

[90] B. Huang, J. Piper, S. Peng, et al., "Magnetostratigraphic study of the Kuche depression, Tarim Basin, and Cenozoic uplift of the Tian shan range, Western China," *Earth and Planetary Science Letters*, vol. 251, nos. 3–4, pp. 346–364, 2006.

[91] D. Xiang, Z. Zhang, W. Xiao, et al., "Episodic Meso-Cenozoic Denudation of Chinese Tianshan: Evidence from Detrital Apatite fission track and Zircon U–PB data, Southern Junggar Basin margin, NW China," *Journal of Asian Earth Sciences*, vol. 175, May, pp. 199–212, 2019.

[92] C. Guo, Z. Zhang, M. G. Malusà, et al., "Late Cenozoic topographic growth of the South Tianshan mountain range: Insights from Detrital Apatite fission-track ages, northern Tarim Basin margin, NW China," *Journal of Asian Earth Sciences*, vol. 234, August, p. 105277, 2022.

[93] Y. Wang, J. Zhang, X. Huang, and Z. Wang, "Cenozoic Exhumation of the Tianshan as constrained by regional low-temperature Thermochronology," *Earth-Science Reviews*, vol. 237, February, p. 104325, 2023.

[94] Y. Chen, S. Gilder, N. Halim, J. P. Cogné, and V. Courtillot, "New Paleomagnetic constraints on central Asian Kinematics: Displacement along the Altyn Tagh fault and rotation of the Qaidam Basin," *Tectonics*, vol. 21, no. 5, pp. 6–1, 2002.

[95] H. P. Zhang, M. E. Oskin, J. Liu-Zeng, P. Zhang, P. W. Reiners, and P. Xiao, "Pulsed Exhumation of interior Eastern Tibet: Implications for relief generation mechanisms and the origin of high-elevation Planation surfaces," *Earth and Planetary Science Letters*, vol. 449, September, pp. 176–185, 2016.

[96] Y. Tian, R. Li, Y. Tang, X. Xu, Y. Wang, and P. Zhang, "Thermochronological constraints on the late Cenozoic Morphotectonic evolution of the min shan, the Eastern margin of the Tibetan plateau," *Tectonics*, vol. 37, no. 6, pp. 1733–1749, 2018.

[97] W. Wang, P. Zhang, C. N. Garzione, et al., "Pulsed rise and growth of the Tibetan plateau to its northern margin since ca. 30 ma," *Proceedings of the National Academy of Sciences of the United States of America*, vol. 119, no. 8, 2022.

[98] A. Yin, "Cenozoic Tectonic evolution of Asia: A preliminary synthesis," *Tectonophysics*, vol. 488, nos. 1–4, pp. 293–325, 2010.

[99] J. Yin, W. Chen, K. V. Hodges, et al., "The thermal evolution of Chinese central Tianshan and its implications: Insights from multi-method Chronometry," *Tectonophysics*, vol. 722, January, pp. 536–548, 2018.

[100] Z. Zhang, W. Zhu, L. Shu, et al., "Multi-stage Exhumation of the NE Tarim Precambrian bedrock, NW China: Constraints from Apatite fission track Thermochronology in the Kuluketage area," *Terra Nova*, vol. 23, no. 5, pp. 324–332, 2011.

[101] Z. Zhang, W. Zhu, D. Zheng, B. Zheng, and W. Yang, "Apatite fission track Thermochronology in the Kuluketage and Aksu areas, NW China: Implication for Tectonic evolution of the northern Tarim," *Geoscience Frontiers*, vol. 7, no. 2, pp. 171–180, 2016.

[102] E. R. Sobel, M. Oskin, D. Burbank, and A. Mikolaichuk, "Exhumation of basement-cored uplifts: Example of the Kyrgyz Range quantified with apatite fission track thermochronology," Tectonics, vol. 25, no.2, p. TC2008, 2006.

[103] S. Glorie, J. De Grave, M. M. Buslov, et al., "Tectonic history of the Kyrgyz South Tien shan (Atbashi-Inylchek) Suture zone: The role of inherited structures during deformation-propagation," *Tectonics*, vol. 30, no. 6, p. n, 2011.

[104] E. A. Macaulay, E. R. Sobel, A. Mikolaichuk, A. Landgraf, B. Kohn, and F. Stuart, "Thermochronologic insight into late Cenozoic deformation in the basement-Cored Terskey range, Kyrgyz Tien shan," *Tectonics*, vol. 32, no. 3, pp. 487–500, 2013. http://doi.wiley.com/10.1002/tect.v32.3.

[105] E. A. Macaulay, E. R. Sobel, A. Mikolaichuk, B. Kohn, and F. M. Stuart, "Cenozoic deformation and Exhumation history of the central Kyrgyz Tien shan," *Tectonics*, vol. 33, no. 2, pp. 135–165, 2014.

[106] Z. Chen, J. Wang, J. Liu et al., "Multi-Stage Uplift and Exhumation of the West Tianshan Mountain: Evidence from the Apatite Fission-Track Dating." Acta Geoscientica Sinica, vol. 27, no.2, pp. 97–106, 2006.

[107] Z. Guo, Z. Zhang, C. Wu, S. Fang, and R. Zhang, "The Mesozoic and Cenozoic Exhumation History of Tianshan and Comparative Studies to the Junggar and Altai Mountains," Acta Geologica Sinica, vol. 80, no.1, pp.1–15, 2006.

[108] Z. Du and Q. Wang, "Mesozoic and Cenozoic Uplifting history of the Tianshan region: Insight from Apatite fission track," *Acta Geologica Sinica*, vol. 81, no. 8, pp. 1081–1101, 2007.

[109] A. Käßner, L. Ratschbacher, R. Jonckheere, et al, "Cenozoic Intracontinental deformation and Exhumation at the Northwestern tip of the India-Asia collision—Southwestern Tian shan, Tajikistan, and Kyrgyzstan," *Tectonics*, vol. 35, no. 9, pp. 2171–2194, 2016.

[110] G. Jepson, S. Glorie, D. Konopelko, et al., "Thermochronological insights into the structural contact between the Tian shan and Pamirs, Tajikistan," *Terra Nova*, vol. 30, no. 2, pp. 95–104, 2018. https://onlinelibrary.wiley.com/toc/13653121/30/2.

[111] A. Bande, E. R. Sobel, A. Mikolaichuk, A. Schmidt, and D. F. Stockli, "Exhumation history of the Western Kyrgyz Tien shan: Implications for Intramontane Basin formation," *Tectonics*, vol. 36, no. 1, pp. 163–180, 2017. http://doi.wiley.com/10.1002/tect.v36.1.

[112] A. Bande, E. R. Sobel, A. Mikolaichuk, and V. Torres Acosta, "Talas–Fergana fault Cenozoic timing of deformation and its relation to Pamir Indentation," *Geological Society, London, Special Publications*, vol. 427, no. 1, pp. 295–311, 2017.

[113] E. R. Sobel, J. Chen, and R. V. Heermance, "Late Oligocene-early Miocene initiation of shortening in the Southwestern Chinese Tian shan: Implications for Neogene shortening rate variations," *Earth and Planetary Science Letters*, vol. 247, nos. 1–2, pp. 70–81, 2006.

[114] S. Yang, H. Chen, X. Cheng et al., "Cenozoic uplifting and unroofing of southern Tien Shan, China," Journal of Nanjing University (Natural Sciences), vol. 39, no.1, pp.1–8, 2003.

[115] Y. Wang, K. Cai, M. Sun, et al., "Tracking the multi-stage Exhumation history of the Western Chinese Tianshan by Apatite fission track (AFT) dating: Implication for the preservation of epithermal deposits in the ancient Orogenic belt," *Ore Geology Reviews*, vol. 100, September, pp. 111–132, 2018.

[116] B. Li, X. Zhuang, J. Li, and S. Zhao, "Geological controls on coal quality of the Yili Basin, Xinjiang, Northwest China," *International Journal of Coal Geology*, vol. 131, September, pp. 186–199, 2014.

[117] L. Shao, K. Stattegger, W. Li, and B. J. Haupt, "Depositional style and subsidence history of the Turpan Basin (NW China)," *Sedimentary Geology*, vol. 128, nos. 1–2, pp. 155–169, 1999.

[118] T. J. Greene, A. R. Carroll, M. S. Hendrix, S. A. Graham, M. A. Wartes, and O. A. Abbink, "Sedimentary record of Mesozoic deformation and inception of the Turpan- Hami basin, northwest China," Geological Society of America Memoir 194, pp. 317–340, 2001.

[119] W. Tang, Z. Zhang, J. Li, K. Li, Z. Luo, and Y. Chen, "Mesozoic and Cenozoic uplift and Exhumation of the Bogda mountain, NW China: Evidence from Apatite fission track analysis," *Geoscience Frontiers*, vol. 6, no. 4, pp. 617–625, 2015.

[120] Y.-T. Yang, C.-C. Song, and S. He, "Jurassic Tectonostratigraphic evolution of the Junggar Basin, NW China: A record of Mesozoic Intraplate deformation in central Asia," *Tectonics*, vol. 34, no. 1, pp. 86–115, 2015.